CAMS Service Evolution

D1.7 Report on improved retrievals for IFS-AER and evaluation of global CAMS products

Due date of deliverable	30-Nov-25
Submission date	18-Dec-2025
File Name	CAMEO-D1-7-V1.0
Work Package /Task	WP1 T1.7
Organisation Responsible of Deliverable	TNO
Author name(s)	Jessie Zhang, Xinya Liu, Janot Tokaya, Arjo Segers
Revision number	V1.0
Status	Issued
Dissemination Level	Public

Funded by the European Union

The CAMEO project (grant agreement No 101082125) is funded by the European Union.
Views and opinions expressed are however those of the author(s) only and do not necessarily reflect those of the European Union or the Commission. Neither the European Union nor the granting authority can be held responsible for them.

1 Executive Summary

Aerosols play a crucial role in many atmospheric processes such as chemistry, radiation balances, and cloud formation. For air quality, aerosols are important because of their adverse effects on human health. The wavelength-dependent interactions between aerosols and radiation are quantified by column-integrated bulk optical properties like aerosol optical depth (AOD), single scattering albedo (SSA), and asymmetry parameter (ASY), as well as three-dimensional diagnostics such as extinction and backscatter coefficients.

The ECMWF's Integrated Forecasting System (IFS) provides these diagnostics in forecasting mode and assimilates satellite-retrieved AODs at 550 nm from MODIS and VIIRS (since 2023) as well as from AATSR Envisat (2003-2012) in a reanalysis system. Based on modelled aerosol mass mixing ratios (MMRs), the optical diagnostics are computed. Incorporating observations aims to bring modelled results closer to reality. For optical diagnostics, it is possible to align measured and modelled results for assimilated quantities, such as AOD, while introducing greater discrepancies in underlying fields, such as aerosol concentrations. For example, when modelled aerosol fields are optically less active than in reality, total aerosol concentrations or emissions are perturbed to match ground and satellite retrieved AODs. The existing assimilation schemes generally rely on limited input data such as single-wavelength AOD, which does not contain sufficient information on aerosol speciation. In addition, various parameterizations for individual aerosols like size, scattering properties and mixing state contributes to model uncertainties, presenting difficulties in translating optical observations to the model state of mass concentration. Therefore, it is crucial to have an accurate optical representation of aerosols to maximize the benefit of assimilating optical diagnostics, evaluate sensitivities of various aerosol characteristics, and quantify the model uncertainties in time and space.

Testing the optical representation of aerosols in the IFS model and the sensitivities therein can be performed independently from the IFS model in a standalone offline Observation-Offline-Optical-Post-Processor (OOPP). Such a tool enables quick calculations because it avoids the necessity to calculate (nearly) independent processes like transport and chemistry. As result, OOPP is able to produce aerosol optical ensemble results for testing various assimilation setups. This tool has been developed in the CAMEO project and is described in deliverable D1.6. As mentioned in CAMEO deliverable D1.4, there are inconsistencies between aerosol optical properties used in various remote sensing algorithms (both for satellite and ground-based observations of aerosol optical diagnostics) and in global circulation and chemical transport models such as IFS. Aerosols are represented with different optical properties, sizes, and modal distributions. To be able to quickly test the effect of the selected optical representations, the offline optical operator has shown to be a useful tool.

OOPP has demonstrated its ability to evaluate and improve the optical representation of aerosols in the IFS model, including SSA and AOD. Analysis of the current CAMS global reanalysis (EAC4)found overall good agreement compared to AOD of AERONET and SPEXone, albeit with overestimation in biomass-burning regions and high uncertainties from wet organic matter. SSA, however, shows an underestimation over land globally, and CAMS EAC4 reanalysis has difficulty capturing SSA variability. Multiple experiments were conducted to simulate AOD and SSA. Increasing SSA, especially for organic matter (OM), decreases the bias. The dust and sea salt optical schemes do not contribute much in terms of global AOD. The dust scheme based on Dubovik (2006) shows better agreement in SSA than the scheme based on Woodward (2001), which was used as default for EAC4. Experiments showed that simulated AOD and SSA at multiple wavelengths is especially sensitive for the amount of organic matter. Based on this it is proposed that assimilation of AOD at multiple wavelengths should change mass mixing ratios of organic matter separate from the other aerosols, while currently the AOD assimilation using single-wavelength setup does not differentiate the aerosols compositions.

Table of Contents

List of abbreviations

Abbreviation	Full Term
ADS	Atmosphere Data Store
AERONET	Aerosol Robotic Network (ground-based remote sensing aerosol system)
AOD	Aerosol Optical Depth (also referred to as Aerosol Optical Thickness, AOT)
AAOD	Absorption Aerosol Optical Depth
AOT	Aerosol Optical Thickness (see AOD)
ASY	Asymmetry parameter
BC	Black Carbon
CAMS	Copernicus Atmosphere Monitoring Service
CAMEO	CAMS EvOlution
CY48R1	IFS model cycle 48 release 1
EAC4	CAMS Global Reanalysis (Atmospheric Composition)
EGG4	CAMS Global Greenhouse Gas Reanalysis
ERA5	ECMWF Reanalysis v5
IFS	Integrated Forecasting System
IFS-AER	Integrated Forecasting System aerosol scheme
IPCC	Intergovernmental Panel on Climate Change
LUT	Look-Up-Table
MARS	ECMWF Meteorological Archival and Retrieval System
MEC	Mass Extinction Coefficient
MLE	Maximum Likelihood Estimation
MMR	Mass Mixing Ratio
MNB	Mean Normalized Bias
NIR	Near Infrared
OOPP	Offline-Optical-Post-Processor
OPAC	Optical Properties of Aerosols and Clouds
OM	Organic Matter
RH	Relative Humidity
RMSE	Root Mean Square Error
SPEXone	Spectro-polarimeter for Planetary EXploration one
SSA	Single Scattering Albedo
VCD	Vertical Column Density
WOM	Hydrophilic/wet organic matter
4DVar	4D variational Data Assimilation

2 Introduction

2.1 Background

Monitoring the composition of the atmosphere is a key objective of the European Union's flagship Space programme Copernicus, with the Copernicus Atmosphere Monitoring Service (CAMS) providing free and continuous data and information on the atmospheric composition including aerosol concentrations.

As mentioned in CAMEO deliverable D1.4, currently, there are inconsistencies between aerosol optical properties used in various remote sensing retrieval algorithms (both for satellite and ground-based observations of aerosol optical diagnostics) and in the climate and chemical transport models such as IFS. Aerosols are represented with different optical properties, and sizes distributions for the various chemical components. However, producing optical diagnostic parameters for atmospheric aerosol by running chemical transport models including optical calculations can be computationally extensive work. An Offline-Optical-Post-Processor (OOPP), was developed for IFS-AER to enable quick calculations of optical diagnostics from aerosol mass mixing ratios (MMRs). This tool is used to evaluate the uncertainty of global CAMS optical products with remote sensing observations and prepare the assimilation of novel observations. The tool is specifically useful for quick calculations of optical diagnostics and thereby allows testing of different optical properties, calculate sensitivities and explore alternative optical diagnostics.

The aerosols in the IFS model, which in the data used in this study comprise of 11 species (three size bins for dust and sea salt, hydrophilic and hydrophobic black carbon and organic matter and sulphate, as used to produce the CAMS Reanalysis), are also compared to (speciated) ground measurements of aerosol concentrations. This comparison is not a topic of the work presented here where the focus lies on the evaluation of (column integrated) optical diagnostics of the atmosphere.

OOPP and its evaluation are described in deliverable D1.6. The data flow of the operator is illustrated in Figure 2-1.The bulk optical properties of aerosols are assumed independent from the physical and chemical processes that govern their lives in the atmosphere, so aerosol MMRs can be translated directly into optical diagnostics.

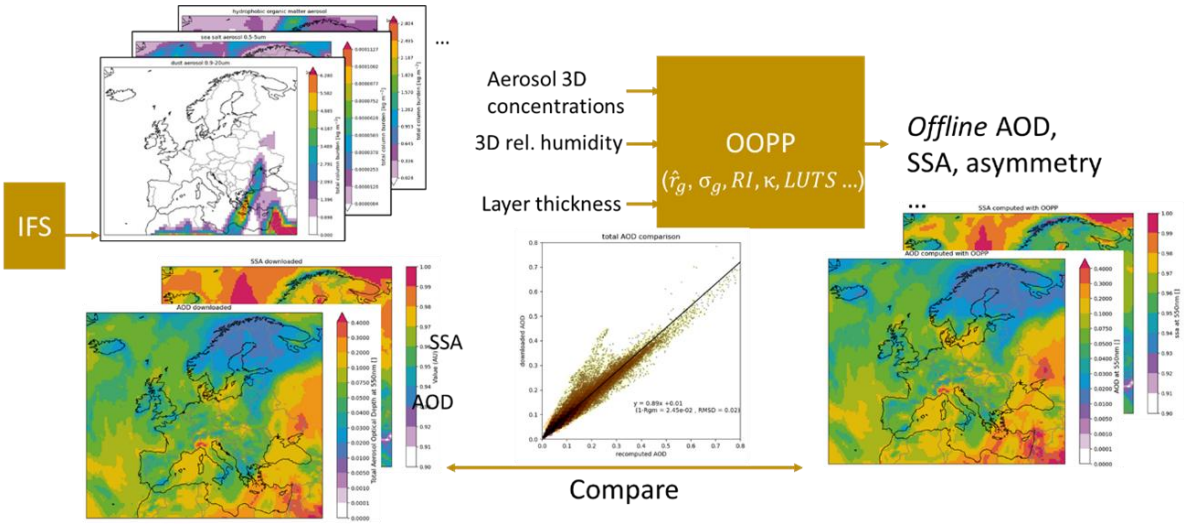

Figure 2-1 Illustration of OOPP showing inputs and outputs.

The optical properties of aerosols are usually calculated using Mie scattering, which describes how electromagnetic waves interact with dielectric spheres. These interactions depend on the microscopic properties of the sphere, e.g., complex refractive index and size with respect to the wavelength of the radiation. Thus, aerosol bulk optical properties can be derived from Mie calculations under the assumption that aerosols can be represented as a population of dielectric spheres. In most chemical transport models, including the IFS, representative bulk mass extinction coefficients (MECs), single scattering albedos (SSAs), and asymmetry parameters (ASYs) are determined and used to translate MMRs into overall optical diagnostics. This is based on assumptions on size distributions and dielectric properties for each aerosol species. The results of the Mie calculation are usually stored in a look-up-table (LUT) for computational efficiency.

Various representations of aerosol bulk optical properties are stored in LUTs. For the hydrophilic aerosols, 12 different relative humidity (RH) ranges are stored to account for differences in aerosol water content. These values are based on assumptions on aerosol and water refractive index, size distribution, and water affinity. The precomputed bulk optical properties are AOD, SSA and ASY. These properties are used to simulate equivalent optical diagnostic properties of the atmosphere. Satellite and ground-based remote sensing measurements probe the atmosphere and produce observation data. This observed data can be used to assess model accuracy, and these three optical diagnostics provide different information content.

AOD (or Aerosol optical thickness, AOT) is a measure of how much light is attenuated upon propagation through the atmosphere due to scattering and absorption by aerosols. This is an extrinsic property dependent on the total column mass of aerosol (burden) in the atmosphere and the aerosol extinction efficiency. Because it is dependent on these two properties, there are two approaches to bring observations and model results into closer agreement. Most aerosols transport modelling and associated data assimilation systems analyse AOD bias and accuracy with respect to observations by altering modelled aerosol masses (Garrigues et al., 2023). In this work we have tested both the mass description (mainly size partitioning) and the optical representation of various aerosols species.

SSA is an intrinsic measure (not dependent on total column aerosol mass) and is given by the ratio between extinction and absorption of radiation. SSA remains highly uncertain, partly due to limited spatial observations previously and limited focus in literature compared to AOD. Nevertheless, SSA is an important aerosol optical diagnostic parameter that influences aerosol direct radiative forcing. In general, when SSA > 0.85 the aerosol radiative forcing would be negative (cooling effect), and vice versa (Takemura et al., 2002). Yet, compared to AOD there is limited study investigating global modelled SSA and observation which leaves the aerosol direct radiative effect as climate forcing is highly uncertain (current estimate of forcing is 1.3 W/m^2, IPCC AR6). Since OOPP can quickly test different optical assumption for aerosols and produce AOD and SSA, we have experimented with various optical properties of different aerosol species and examined these through comparisons with observations.

ASY is also an intrinsic measure and describes directional scattering of radiation, ranging from -1 (completely backwards) to +1 (completely forwards). It is a crucial factor in climate and atmospheric science for determining direct aerosol radiative forcing. As ASY describes the directionality of scattering of radiations, it is directly related to the aerosol phase function and impacts aerosol albedo. ASY depends primarily on the particle size, with larger particles scattering more light forward leading to higher ASY values. If ASY is high, it means more light scattering forwards resulting in less cooling effect and vice versa. Hence, a combination of SSA and ASY could explain the aerosol direct effects on radiation.

Next to the evaluation of these less customarily compared optical diagnostics (SSA and ASY) and the testing of various optical representations of the aerosols, OOPP is exploited to gain insights into the sources of uncertainty in the AOD using a maximum likelihood estimation, which requires quantification of the effect of (small) perturbations to the aerosol

concentrations. This information can be used to design future assimilation systems that also benefit from information on spatial and temporal correlation lengths in the aerosol field. The latter topic will also be briefly discussed in this deliverable.

2.2 Scope of this deliverable

2.2.1 Objectives of this deliverables

OOPP is applied in a multitude of experiments on IFS aerosol concentration data to test various aerosol representations and explore sensitivities within the aerosol description. OOPP is used to analyse difference between CAMS-OOPP and remote sensing observation products (AERONET and SPEXone). Tests are performed to see which uncertainties might explain the differences between model and measurements by changing aerosol masses, aerosol type partitioning and optical properties.

Secondly the IFS AOD data is used to formulate spatial and temporal correlation lengths scales and test sensitivities using maximum likelihood estimates.

2.2.2 Deviations and counter measures

No deviations have been encountered.

2.2.3 CAMEO Project Partners

ECMWF	EUROPEAN CENTRE FOR MEDIUM-RANGE WEATHER FORECASTS
Met Norway	METEOROLOGISK INSTITUTT
BSC	BARCELONA SUPERCOMPUTING CENTER-CENTRO NACIONAL DE SUPERCOMPUTACION
KNMI	KONINKLIJK NEDERLANDS METEOROLOGISCH INSTITUUT
SMHI	SVERIGES METEOROLOGISKA OCH HYDROLOGISKA INSTITUT
BIRA-IASB	INSTITUT ROYAL D'AERONOMIE SPATIALEDE BELGIQUE
HYGEOS	HYGEOS SARL
FMI	ILMATIETEEN LAITOS
DLR	DEUTSCHES ZENTRUM FUR LUFT - UND RAUMFAHRT EV
ARMINES	ASSOCIATION POUR LA RECHERCHE ET LE DEVELOPPEMENT DES METHODES ET PROCESSUS INDUSTRIELS
CNRS	CENTRE NATIONAL DE LA RECHERCHE SCIENTIFIQUE CNRS
GRASP-SAS	GENERALIZED RETRIEVAL OF ATMOSPHERE AND SURFACE PROPERTIES EN ABREGE GRASP
CU	UNIVERZITA KARLOVA

CEA	COMMISSARIAT A L ENERGIE ATOMIQUE ET AUX ENERGIES ALTERNATIVES
MF	METEO-FRANCE
TNO	NEDERLANDSE ORGANISATIE VOOR TOEGEPAST NATUURWETENSCHAPPELIJK ONDERZOEK TNO
INERIS	INSTITUT NATIONAL DE L ENVIRONNEMENT INDUSTRIEL ET DES RISQUES - INERIS
IOS-PIB	INSTYTUT OCHRONY SRODOWISKA - PANSTWOWY INSTYTUT BADAWCZY
FZJ	FORSCHUNGSZENTRUM JULICH GMBH
AU	AARHUS UNIVERSITET
ENEA	AGENZIA NAZIONALE PER LE NUOVE TECNOLOGIE, L'ENERGIA E LO SVILUPPO ECONOMICO SOSTENIBILE

3 Methods

3.1 Model Description and OOPP

The experiments described in this document are performed with OOPP based on IFS model cycle 48 release 1 (CY48R1). This model version uses a LUT that contains ensemble integrated optical properties of individual aerosol species. As described in more detail in CAMEO deliverable D1.6, OOPP is based on the optical routines in the IFS model. It calculates optical diagnostics of the atmosphere, based on the aerosol MMRs and meteorological inputs (temperature, pressure and specific humidity).

The optical routines can be relatively easily tailored for specific experiments. This capability has been used to change the optical representation of various aerosols, the mass partitioning in various aerosol sizes, SSA representations and the sensitivity with respect to relative humidity (RH). OOPP can produce output on the input grid, i.e. on the same resolution and coverage as the input files, or on a list of locations of interest provided to OOPP. The latter option was used to calculate optical diagnostics on selected AERONET site locations.

3.2 IFS reanalysis dataset

In this study we have used data from the CAMS global reanalysis (EAC4; Inness et al. 2019) that covers the period 2003 - December 2024 and contains the aerosol MMRs for the aerosols listed in Table 1.

The EAC4 is the latest global reanalysis data set of atmospheric composition (AC) produced by ECMWF, and consists of 3-dimensional time-series of mass mixing ratio's. The CAMS reanalysis was produced using 4DVar data assimilation in CY42R1 of ECMWF's IFS, with 60 hybrid sigma/pressure (model) levels in the vertical, with the top level at 0.1 hPa. The full data set (on model layers) is archived in the ECMWF Meteorological Archival and Retrieval System (MARS), but a subset (on pressure levels) could also be obtained from Atmosphere Data Store (ADS).

The 4DVar data assimilation uses 12 hour assimilation windows from 09 UTC to 21 UTC and 21 UTC to 09 UTC. The IFS model documentation for various model cycles can be found online[1]. The model used in the CAMS reanalysis includes several updates to the aerosol and chemistry modules on top of the standard CY42R1 release[2].

[1] https://www.ecmwf.int/en/publications/ifs-documentation
[2] https://confluence.ecmwf.int/display/CKB/CAMS%3A+Reanalysis+data+documentation

Table 1 - IFS data used by OOPP and collected from the Atmospheric Data Store (ADS).

Aerosol names	**Variable name in ADS [units]**
Dust aerosol (0.03 - 0.55 µm) mixing ratio*	dust_aerosol_0.03-0.55um_mixing_ratio [kg kg^{-1}]
Dust aerosol (0.9 - 20 µm) mixing ratio*	dust_aerosol_0.9-20um_mixing_ratio [kg kg^{-1}]
Dust aerosol (0.55 - 0.9 µm) mixing ratio*	dust_aerosol_0.55-0.9um_mixing_ratio [kg kg^{-1}]
Hydrophilic black carbon aerosol mixing ratio*	hydrophilic_black_carbon_aerosol_mixing_ratio [kg kg^{-1}]
Hydrophilic organic matter aerosol mixing ratio*	hydrophilic_organic_matter_aerosol_mixing_ratio [kg kg^{-1}]
Hydrophobic black carbon aerosol mixing ratio*	hydrophobic_black_carbon_aerosol_mixing_ratio [kg kg^{-1}]
Hydrophobic organic matter aerosol mixing ratio*	hydrophobic_organic_matter_aerosol_mixing_ratio [kg kg^{-1}]
Sea salt aerosol (0.03 - 0.5 µm) mixing ratio*	sea_salt_aerosol_0.03-0.5um_mixing_ratio [kg kg^{-1}]
Sea salt aerosol (0.5 - 5 µm) mixing ratio*	sea_salt_aerosol_0.5-5um_mixing_ratio [kg kg^{-1}]
Sea salt aerosol (5 - 20 µm) mixing ratio*	sea_salt_aerosol_5-20um_mixing_ratio [kg kg^{-1}]
Sulphate aerosol mixing ratio*	sulphate_aerosol_mixing_ratio [kg kg^{-1}]
Meteo variable names	**Variable name in ADS [units]**
Specific humidity (3D)	specific_humidity [kg kg^{-1}]
Temperature (3D)	temperature [K]
Surface pressure (2D)	surface_pressure [Pa]

3.3 AERONET ground-based observations

The AERONET data comes from a network of ground-based remote sensing aerosol systems. It is considered the gold standard when it concerns optical diagnostics of the atmosphere such as AOD and is often used to validate and/or calibrate models and satellite measurements of equivalent quantities.

In this work AERONET data has been collected for the years 2023 and 2024 to determine and quantify the agreement between model and measurements. Here level 2.0 data from the direct sun algorithm (version 3) was used. To match the temporal resolution of OOPP model outputs, AOD, SSA, and ASY at various wavelengths (340, 440, 550, 670, 865nm) were averaged over three-hour periods, each containing a minimum of three valid observations. Comparisons were made using the wavelengths closest to those used in the OOPP model.

Within the retrieval algorithm of AERONET, model data and aerosol assumptions are introduced to derive optical diagnostics like SSA and ASY. The absorptions for ozone and water vapor are specified using data of Modern-Era Retrospective analysis for Research and Applications, Version 2 (MERRA-2) and NCEP/NCAR reanalysis data, respectively (e.g., Saha et al., 2010). Daily AOD at 550nm are obtained from MERRA-2 assimilation model simulations (Gelaro et al., 2017). The aerosol parametrizations are described in detail in Dubovik & King, 2000 and Dubovik et al., 2006. Basically, a lognormally distributed ensemble of spherical and spheroidal aerosols with a refractive index within a given range, is used to fit the measured spectrally and angularly varying observed intensity of scattered solar radiation. In short, the wavelength dependent AOD and sky radiances are directly measured and used as an input to the retrieval algorithm. Other aerosol diagnostics such as SSA, absorption AOD, asymmetry factors are calculated from the retrieved aerosol column-integrated size distributions and complex refractive indices.

AERONET contains sites that represent a wide range of location types. However, given the resolution and constrains of the IFS model in capturing local emission events, representative background aerosol sites were selected for analysis. Site selection was based on the criteria described by Schutgens et al., 2020, with a relative spatial representation error below 20% for either AOT or AAOT. The sites that are assumed to be representative for background concentrations are shown in Figure 3-1.

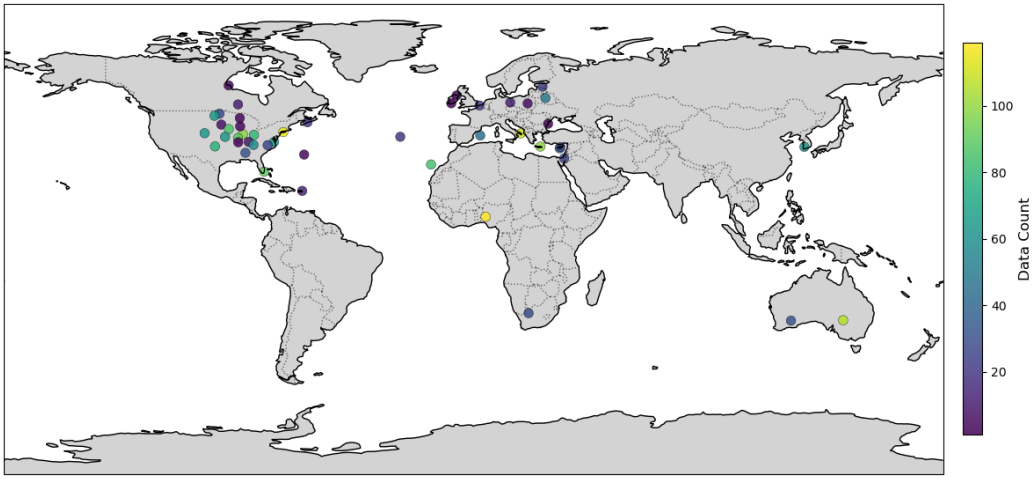

Figure 3-1 - AERONET sites representative for background concentrations based on IFS data.

3.4 Satellite observations of optical diagnostics from SPEXone

SPEXone is a Spectro-polarimeter for Planetary Exploration on the Plankton, Aerosol, Cloud, ocean Ecosystem (PACE) satellite. It was launched in polar orbit in 2024 and starting to provide level 2 data from April 2024. During this study EAC4 was available until the end of 2024 only, and therefore comparison with SPEXone retrievals was done for the overlapping period April-December 2024. Data from SPEXone has been filtered with χ^2 <= 5 on land and χ^2<= 10 on ocean to remove residual cloud contamination (Fu et al., 2025). The orbits of SPEXone have spatial coverage of about 100 km at a native resolution of 5.4 x 4.6 km.

OOPP output of 3 hourly EAC4 data at 0.75ºx0.75º resolution was co-located with the SPEXone retrieval using nearest time and linear spatial interpolation. SPEXone observes 34 wavelengths between 407nm and 749nm on both land and ocean, but the level 2 product retrieval provides wider spectra. We have chosen the common bands between the available lookup table wavelengths in IFS CY48R1 and SPEXone level 2 data which results in a selection of 340, 355, 380, 330, 500, 532, 550, 670, 865, 1020, 1064 nm for further analysis. All level 2 data of SSA and AOT after filtering was collected. OOPP output of vertical column AOD and SSA based on gridded 3 hourly EAC4 data is co-located with retrieved L2 data by nearest time and linear interpolation in 2D surface. For some of the data visualization, data was gridded to 1ºx1º and averaged monthly if not stated otherwise.

3.5 Experiment setup and uncertainty estimation

As mentioned in the introduction, experiments have been conducted to test various parts of the aerosol representation in the IFS model. Table 2 summarises the various experiments, identified by abbreviations that are used in the following sections and figures. The table also indicates weather validation was performed using AERONET or SPEXone (or both).

In terms of burden, dust is one of the most important aerosol species (Bozzo et al., 2017; Gliß et al., 2021). Also, dust has relatively uncertain optical properties due to varying shapes and mineralogical composition. Therefore, in the IFS LUTs multiple optical properties are available for dust. Thereafter, the first set of three of experiments were performed to test three dust representations: The original (Woodward, 2001), a description by Dubovik et al., 2002, and “Composite” dust (Balkanski et al., 2007; Di Biagio et al., 2017; Ryder et al., 2018). A summary of the dust optical properties is shown in Figure 4-4.

In addition to testing these representations, six experiments have been performed with increasing or reducing the MEC values of the default setup (Woodward) by 25% for the three dust sizes. A third set of tests on the dust description concerns the partitioning of the mass into the different size ranges. In this set of experiments, the total mass remains fixed, but 25% of the mass from one size bin is moved to an adjacent bin. Summarizing, the dust description in the IFS model is tested with a total of 13 tests: three descriptions, six MEC changes, and four alternative mass partitionings.

Moreover, sensitivity experiments with SSA properties for the different aerosols species have been conducted. In these experiments, simulations have been compared with SPEXone data over land. First the impact of the different dust optical descriptions on SSA was evaluated. Then, the sensitivity of SSA for black-carbon and organic-matter was tested by keeping the mass mixing ratio (MMR) constant while increasing SSA with 0.2% and 0.4% for organic-matter (both hydrophilic/wet and hydrophobic/dry types), or doubled SSA for black-carbon. In addition, we have also tested moving 25% of the black-carbon mass to organic-matter. Finally, the combined effects of these multiple experiments were also evaluated.

Table 2 - Overview of all experiments.

Abbreviation	AERONET	SPEXone
Dust representations		
Original/Woodward	Woodward	
Dubovik/Du	Dubovik	
Composite	Composite	
Dust mass partitioning		
25u2f	25% dust ultra fine to fine	NA
25f2u	25% dust fine to ultra fine	
25f2c	25% dust fine to coarse	
25c2f	25% dust coarse to fine	
Dust MEC values		
125u; 125f; 125c	+25% dust MEC ultra fine; fine; coarse	NA
075u; 075f; 075c	-25% dust MEC ultra fine; fine; coarse	
Sea salt MEC values:		
075u; 075f; 075c	-25% sea salt MEC ultra fine; fine; coarse	NA
Water uptake		
RH+P10	+10% Relative Humidity	NA
RH-P10	-10% Relative Humidity	
SSA focused		
OM2p	OM SSA+ 0.2%	
OM4p	OM SSA +0.4%	
2xBC	BC double SSA	
BC25toOC	BC mass to OM mass by 25%	
2xBC_OM4P	BC double SSA &OM SSA +0.4%	
DU_2xBC_OM4P	Dust-Dubovik & BC double SSA & OM SSA +0.4%	

4 Results

This section presents the results of the sensitivity experiments conducted to assess aerosol optical depth (AOD) and single scattering albedo (SSA). The evaluation integrates global observations from both ground-based AERONET stations and satellite SPEXone instruments, along with a comprehensive analysis across a few selected regions. Multispectral analyses have been performed at five distinct wavelengths for AERONET and at eleven wavelengths for SPEXone Level 2 retrievals, providing detailed insight into the performance of AOD and SSA across various sensitivity experiments. Table 3 summarises the sensitivity of different aerosol optical configurations, including dust representation, dust size, variations in organic matter (OM) and black carbon (BC) properties, and hygroscopic growth by perturbing RH.

Table 3 - Overview of sensitivity experiments on optical diagnostics. The experiments that show bigger differences will be further elaborated in results and discussion sections. Experiments that showed low sensitivity in the AERONET comparison are not tested further with SPEXone data. Orange text indicates a slight increase in correlation, whereas greenish text indicates a slight decrease.

Abbreviation	Impact on optics	Sections
Dust representations **Original/Woodward** **Dubovik/Du** **Composite**	AOD: Woodward and Dubovik nearly identical, Composite slightly lower SSA: Dubovik better as Woodward shows no correlation with observation ASY: Woodward slightly better	Section 4.1.1 (AERONET) Section 4.3 (SPEXone SSA) Appendix F (SPEXone AOD)
Dust mass partitioning **25u2f** **25f2u** **25f2c** **25c2f**	Mild changes in AOD (675nm) 25u2f: ΔR^2 -0.01 25f2u: ΔR^2 +0.02 25f2c: ΔR^2 +0.00 25c2f: ΔR^2 +0.01	Section 4.2.2
Dust MEC values **125u; 125f; 125c** **075u; 075f; 075c**	Mild changes in AOD (675nm) +25% u/f/c:ΔR^2 +0.02/+0.01/+0.01; -25% u/f/c:ΔR^2 -0.01/-0.01/-0.00;	Section 4.2.2
Sea salt MEC values: **075u; 075f; 075c**	Negligible changes	Appendix C
Water uptake **RH+P10** **RH-P10**	-10% RH: improved AOD correlation (ΔR^2 +0.1 to +0.16 across five wavelengths) +10% RH: decreased AOD correlation (ΔR^2 −0.13 to −0.16 across five wavelengths)	Section 4.2.1 Appendix E

4.1 AERONET AOD and SSA

4.1.1 Comparison of OOPP and AERONET

This section presents a comparison between the AERONET AOD and OOPP model simulations at five wavelengths. For this comparison, the AERONET and model data were matched using the closest available wavelength pairs. Overall, the model and observations show good agreement. R^2 ranges from 0.74 to 0.77, with the highest correlation (0.77) observed near 500 nm and 550 nm. However, the regression slopes display a wavelength dependence. At shorter wavelengths, the model tends to overestimate AOD relative to AERONET, with a slope of 1.09 at 340nm, whereas at longer wavelengths the model underestimates AOD, with a slope of 0.79 at 870nm. This spectral bias likely suggests that the simulated aerosol population consists of smaller particles than observations. By visualizing the relative contributions of hydrophilic/wet organic matter (WOM) through colour and dust through marker size in the scatter plots in Figure 4-1 we found that the OOPP/IFS model overestimates AOD in cases dominated by WOM, whereas it underestimates AOD when dust makes a larger contribution. This pattern is consistent with the overall component distribution shown in Figure A-1 (Appendix A), which presents the relative contributions of individual species to the total AOD at 550 nm in the IFS model. As illustrated, WOM and dust are the two primary contributors to the total AOD at the AERONET sites, and OM accounts for more than 70% on average to the total AOD at 550nm over land globally in the EAC4 CAMS reanalysis dataset.

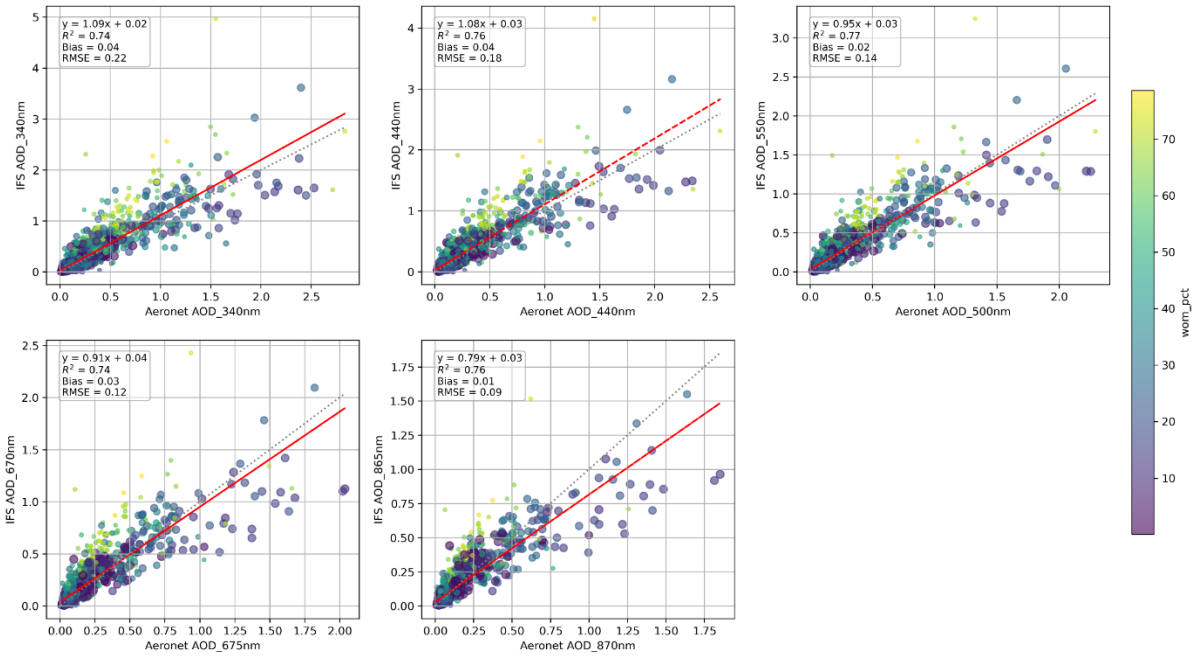

Figure 4-1 - Comparison between AERONET AOD and OOPP model simulations at five wavelengths (340, 440, 500, 675, and 870 nm) for 2023 and 2024. Scatter points are coloured and sized according to the relative contributions of WOM and dust, respectively.

Since the discrepancy between the model and observations appears to originate mainly from the WOM component, the representation of this component in the model is likely the main cause of observed mismatches. These may include misrepresentations in the simulated total concentration of WOM, uncertainties in its hygroscopic growth parameterization, or the use of a single set of hygroscopicity parameter to represent all organic matter species. Such simplifications may fail to capture the diverse humidity responses of different organic aerosol types, leading to systematic biases in AOD. Other contributing factors could include the

inaccurate description of particle size distribution for coarse mode aerosols such as dust and sea salt, which usually show larger impact on AOD at longer wavelengths. So, the impact of dust and sea salt on AOD were tested in the following sections.

For SSA, we found a different pattern compared to AOD, as shown in Figure 4-2. Overall, the discrepancies between the model and observations are larger. Observed SSA values span a wide range, approximately 0.75 to 1.0, whereas the OOPP model simulations vary mostly between 0.8 and 0.85 at 440 nm. This indicates that the model underestimates the variability of SSA at shorter wavelengths. At longer wavelengths, where dust contributions are higher, the bias between model and observations is reduced. However, SSA is significantly underestimated in the model under conditions of high WOM contribution.

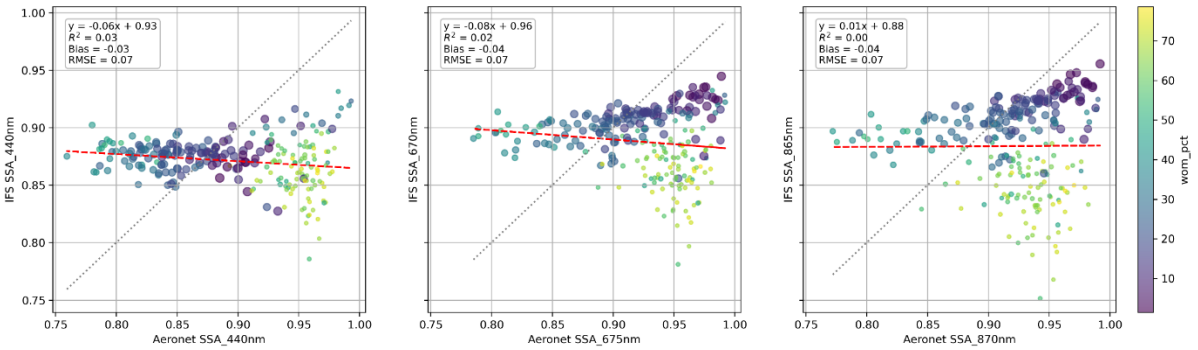

Figure 4-2 - Comparison between AERONET SSA and OOPP model simulations at three wavelengths (440, 675, and 870 nm) for 2023 and 2024. Scatter point colours and sizes follow the same scheme as in Figure 4-1.

In general, this result suggests that the parameterization of WOM in the model is unable to fully capture measured behaviour. In particular, the CAMS EAC4 reanalysis treats all organic matter uniformly and cannot account for differences among various OM types. In addition, SSA discrepancies may also arise from uncertainties in the refractive index or MEC values. However, since the IFS model relies on existing LUTs, further testing of refractive index was not possible within the current framework. However, we conducted additional tests using MEC values, the results of which are presented in the following sections through comparisons between model simulations.

The results for ASY are presented in Figure 4-3. Overall, the model underestimates ASY compared to observations. However, at longer wavelengths, this bias between the model and measurements is reduced, and the correlation improves relative to shorter wavelengths. Since the calculation of ASY is affected by the distribution of AOD and SSA of each species in the IFS model, it is less straightforward to evaluate. We will mainly focus on AOD and SSA in this deliverable, and ASY will only be briefly mentioned.

To further investigate the potential sources of the bias between model and observations, we conducted sensitivity experiments focusing on the impact of relative humidity and the particle size of dust aerosols on aerosol optical properties. These experiments are listed in Table 2 and results are described in section 4.2.

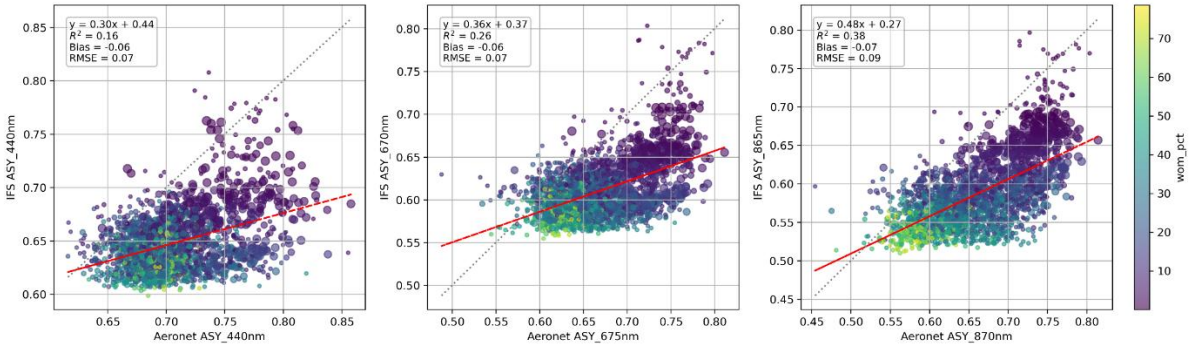

Figure 4-3 - Comparison between AERONET ASY and OOPP model simulations at three wavelengths (440, 675, and 870 nm) for 2023 and 2024. Scatter point colours and sizes follow the same scheme as mentioned in Figures 4-1.

4.1.2 Selection of the description of dust in the IFS lookup tables

As mentioned in section 3.5, we tested dust representation using Woodward, Dubovik, and Composite schemes available in the IFS lookup tables. Figure 4-4 shows MEC and SSA values for these descriptions. The MEC values show that the ultrafine fraction has the highest MEC and the variability between the different descriptions is limited (<20%). The highest SSA is also found in ultrafine dust, with the strongest variability in SSA across the different descriptions occurring at 340nm.

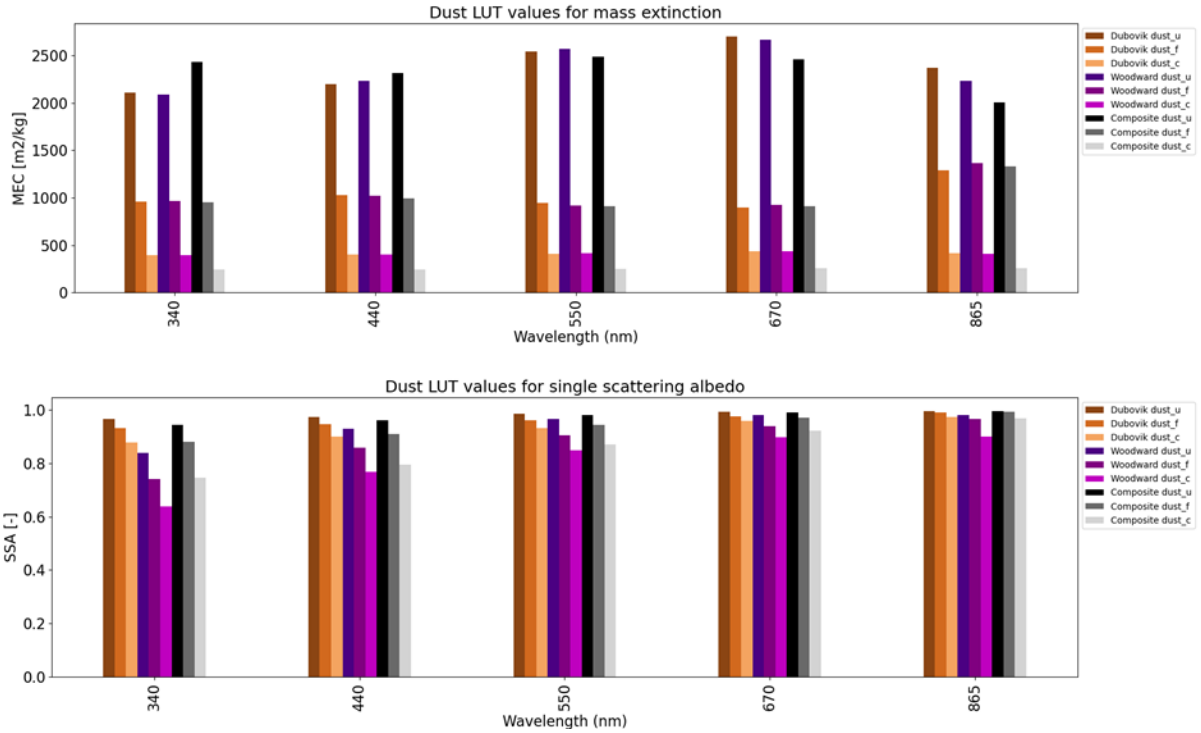

Figure 4-4 - The difference between the MEC (top) and SSA (bottom) values of the dust optical properties in the IFS LUT for the three tested descriptions.

These three dust representations were evaluated against AERONET observations, and the results at 440nm are shown in Figure 4-5. For AOD, the three representations show very similar performance, where the Woodward and Dubovik schemes produce nearly identical results, while the Composite description shows only a minor difference. For SSA, all three representations show less variability compared to AERONET, with the Dubovik scheme having a slightly better correlation than the others. For the asymmetry parameter, ASY, the Woodward scheme demonstrates a slightly higher correlation than the others. However, the agreement between modelled and observed SSA and ASY is generally very low. This is likely due to inaccurate parameterization of SSA and ASY species, or possibly because WOM was treated as a single group, resulting in reduced variability. AOD results are comparable across all three schemes, with Woodward showing slightly better correlations, also for wavelength above 500 nm. Thus, the default Woodward scheme in the IFS model has been applied in OOPP for the subsequent analyses comparing to AERONET.

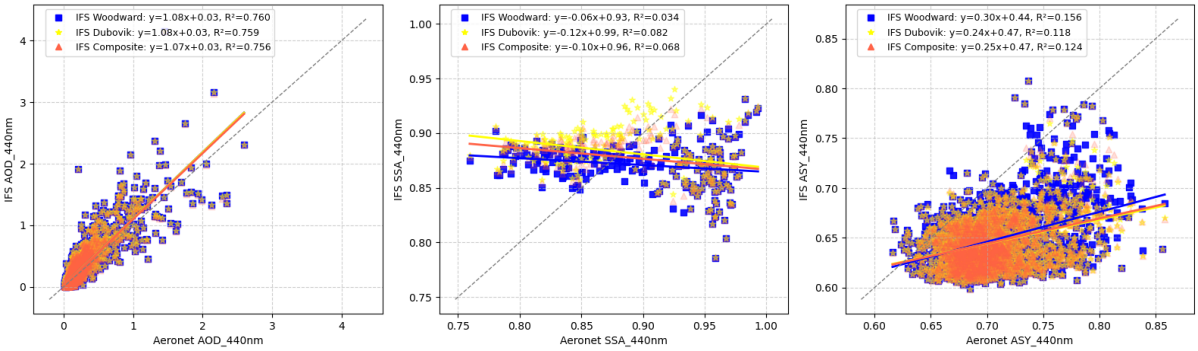

Figure 4-5 - Comparison between AERONET observations and OOPP model simulations with dust representation of Woodward, Dubovik and Composite for AOD, SSA, ASY at 440nm for 2023 and 2024.

4.2 Experiments on Optical diagnostics

4.2.1 Relative humidity/water uptake

We conducted two sensitivity experiments by decreasing and increasing the RH by 10% to evaluate its impact on AOD, as listed in Table 2. The results are presented in Figure 4-6. Reducing the RH by 10% in the model led to an improvement in the correlation between simulated and observed AOD across all wavelengths, whereas increasing RH had the opposite effect. These results indicate that the differences between model and observation is likely due to an overestimation of the hygroscopic growth factor or hygroscopic species in the model, which can cause excessive growth of hygroscopic particles. This leads to larger particle sizes resulting in higher simulated AOD values, particularly at shorter wavelengths. Given the fact that the WOM is the primary contributor to total AOD over most continental regions globally, as described in the previous section, the hygroscopic growth parameterizations and particle size distributions of WOM, may need to be further refined and treated separately.

Increasing RH by 10% led to higher simulated AOD, slightly compensating for the model's original underestimation at longer wavelengths (with the regression slope increasing from 0.80 to 0.82 at 870 nm). However, the correlation with observations became weaker (with R^2 dropping from 0.732 to 0.697), suggesting that the underestimation at longer wavelengths is not purely caused by insufficient hygroscopic growth, but also an underrepresentation of fine mode aerosol in the model. However, for sea salt dominated sites (mass fraction >80%), as shown in Figure B-1 in the appendix B, increasing 10% RH led to an slight increase of the correlation between simulated and observed AOD, but also resulted in higher slope (slopes>1 for wavelength larger than 440nm). This is in line with the assumption that hygroscopic species might be overestimated in the model.

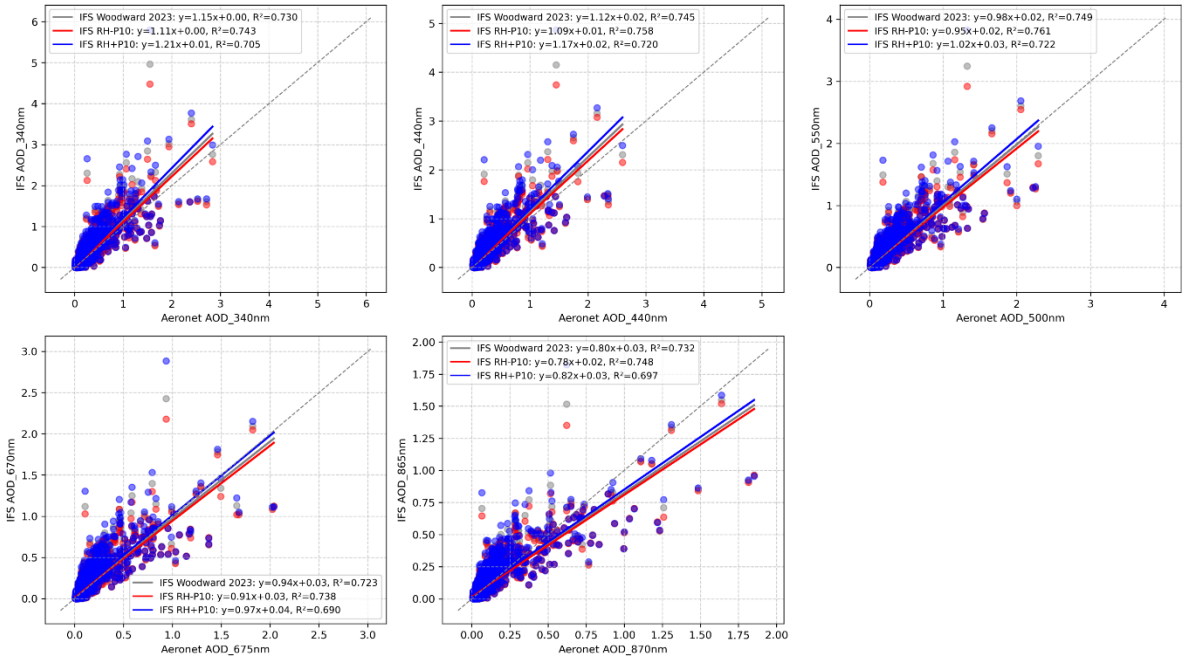

Figure 4-6 - Comparison between AERONET AOD and OOPP model simulations at five wavelengths (340, 440, 500, 675, and 870 nm) for 2023. Gray, blue, and red scatter points represent the original IFS data, simulations with RH decreased by 10%, and simulations with RH increased by 10%, respectively.

The results for the SSA and ASY are presented in Figure B-2 and Figure B-3 in the Appendix B, and exhibit trends comparable to those observed for AOD. Reducing 10% RH leads to a slight decrease in bias between model simulations and observations, along with a small increase in correlations. As these changes are minimal, they may be attributable to a modest improvement in AOD, given that both SSA and ASY are influenced by AOD.

4.2.2 Dust parameters

We conducted ten sensitivity experiments to evaluate the impact of dust mass partitioning in different size bins and MEC values on AOD, as summarized in Table 2. These experiments can be split into two types of perturbations. First, the MEC values of dust in the ultrafine, fine, and coarse modes were increased and decreased by 25%. Second, we adjusted the mass distribution among size modes by shifting the dust mass: 25% from ultrafine to fine, 25% from fine to ultrafine, 25% from coarse to fine, and 25% from fine to coarse. The results are shown in Figure 4-7, where the red box marks the baseline result and the other plots represent the sensitivity experiments. We will use a representative wavelength of 675 nm as a case study, all other wavelengths show similar patterns. The results show that increasing the dust MEC by 25% in each of the three size bins causes a very slightly reduced bias between the model and AERONET observations, with the regression slope increasing from 0.94 to approximately 0.96 and R^2 rising from 0.72 to around 0.74. In contrast, decreasing the MEC values by 25% in each size mode very slightly increases the model and observation discrepancy. In particular, reducing the MEC of the ultrafine mode lowers the slope from 0.94 to 0.91 and R^2 from 0.72 to 0.71. Similar tests were conducted by reducing the sea salt MEC values by 25%, and the results are presented in the appendix C. The results indicate that a 25% reduction in sea salt MEC has a negligible impact on the total AOD at the selected AERONET sites in the period of interest (Figure C-1). Only when sea salt is the dominant component (mass fraction>80%) does a 25% decrease in the fine mode sea salt MEC values lead to approximately 10% reduction in the total AOD (Figure C-2). These results indicate that moderate changes in dust and sea salt MEC have only a minor effect on the model's performance against selected

AERONET sites, mostly over land, suggesting a relatively weak sensitivity of simulated AOD to such perturbations.

Similar patterns were observed in the experiments where the dust mass was shifted among size modes. Shifting 25% of the fine mass to the ultrafine mode or 25% of the coarse mass to the fine mode slightly reduced the discrepancy between the model and observations (with slopes from 0.94 to 0.95-0.98, and R^2 from 0.72 to 0.73-0.74). In contrast, shifting 25% from ultrafine to fine or 25% from fine to ultrafine slightly increased the model and observation discrepancy. The changes suggest that transferring mass from larger to smaller particles tends to improve model performance, likely because fine dust particles (0.55–0.9 μm) contribute more efficiently to light extinction in the visible range, thereby having a similar effect as increasing the MEC. However, the overall impact of these shifts remains very minor. These findings indicate that both mass partitioning and MEC values of the dust and sea salt species have limited potential to bring IFS AODs closer to (the selected) AERONET observations.

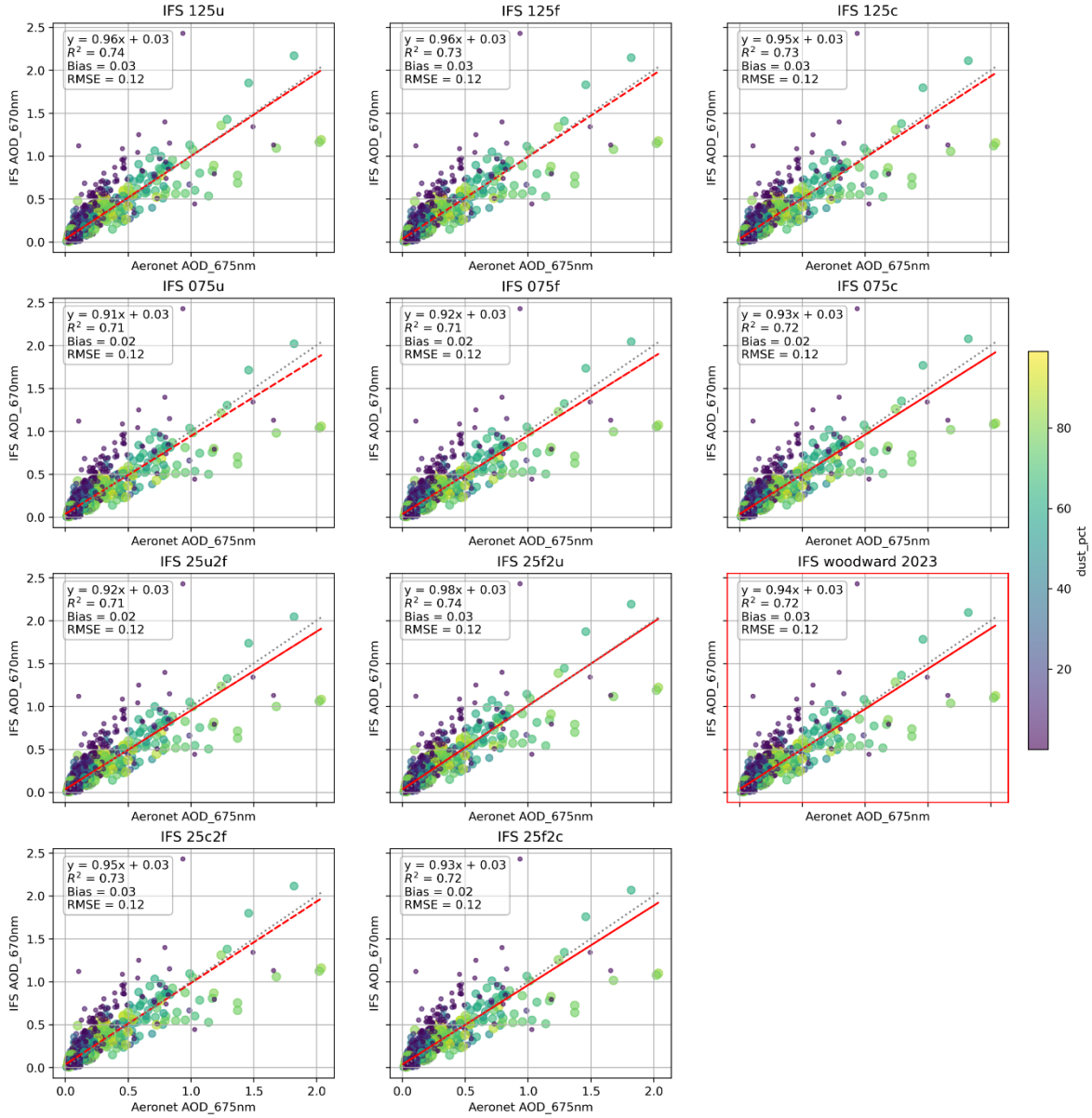

Figure 4-7 - Comparison between AERONET AOD and OOPP model simulations for dust experiments at 675 nm for 2023. Scatter points are coloured and sized according to the relative contributions of dust.

4.3 SPEXone retrieval comparisons with CAMS reanalysis

In this section, EAC4 data is compared with SPEXone retrieved AOD and SSA in 2024. First the global bias is evaluated, followed by a regional analysis for 4 selected regions: the Congo basin, the Canadian peat lands, the Sahara, and northeast India.

4.3.1 Global evaluation

Globally, the OOPP/IFS simulations based on the CAMS EAC4 Reanalysis mass mixing ratios overestimate AOD, except for dust dominated regions. However, it underestimates SSA on land (Figure 4-8), especially in wildfire areas (Siberian forests, Canadian peatlands, and the Congo basin). Comparison with Figure 3-1 shows that in most regions with large positive AOD biases (>0.5) no AERONET stations are available for validation. This is for example the case for the biomass burning regions, but also for densely polluted areas like India. Therefore, SPEXone captures more variation globally over different emission types, especially from natural sources, and is expected to show higher variability than the AERONET analysis. Although the model consistently underestimates SSA at 440nm when compared to SPEXone retrievals on land, the industrial regions in the US, Europe, and Asia exhibit smaller biases than the natural emission-dominated regions on land.

Modelled data show mixed biases over oceans, where hygroscopic growth affects the refractive indices. Notably, underestimation of SSA is centred on the Inter-Tropical Convergence Zone (ITCZ), whereas overestimation occurs outside the ITCZ. These patterns likely result from the advection of continental aerosols and the emission of sulphate aerosols with volcanic origin driven by meteorological and oceanic circulation. As this deliverable mainly focuses on uncertainty in aerosol species on land, ocean locations are not discussed further.

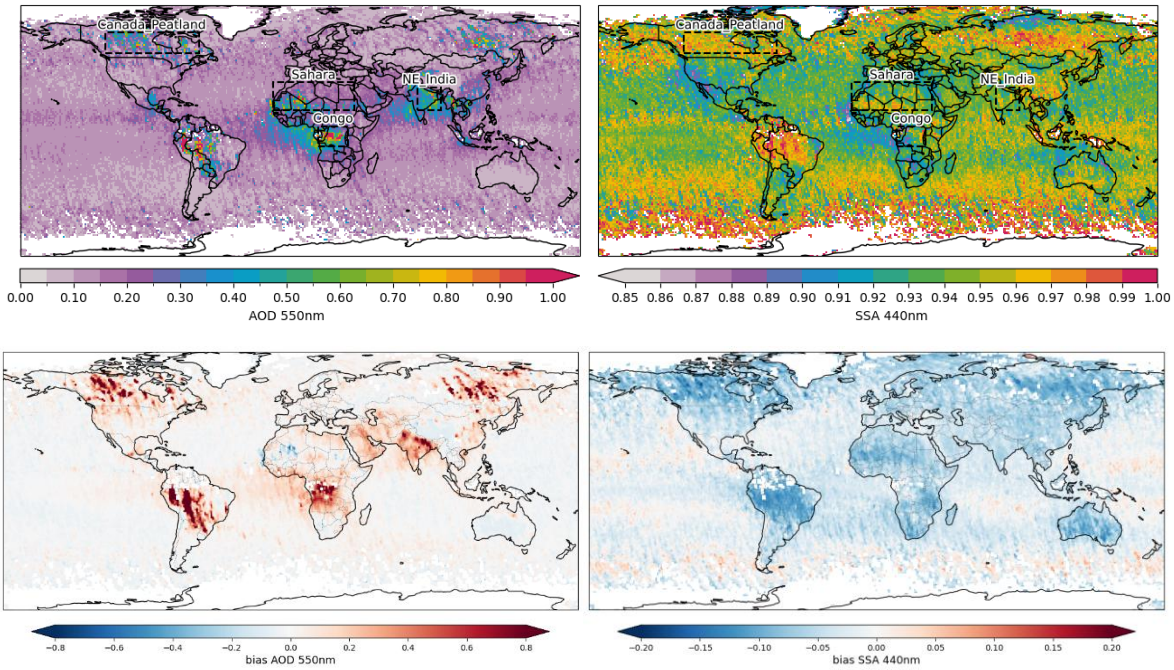

Figure 4-8 - Globally 1°x1° averaged SPEXone retrievals (top) and bias with simulations (bottom) over April-December 2024, for AOD at 550 nm (left) and SSA at 440 nm (right).

Comparison of simulated AOD and SSA with SPEXone retrievals over land shows similar results as seen for AERONET. AOD shows good agreements, with the highest Pearson correlation above 0.8 for wavelengths below 500 nm, decreasing to above 0.6 near 1 μm (Appendix D). In contrast, SSA shows very low correlation (< 0.2) for wavelengths shorter than 700 nm. Although the comparison with SPEXone does not show the highest correlation at 550 nm as seen with AERONET data, differences across the UV and visible ranges are small. The

satellite data, which provide global aerosol optical fields, consistently shows a positive bias with AOD across all wavelengths, unlike some specific AERONET stations. In the deserts, modelled AOD shows an underestimation especially in the Sahara region. However, given the modelled resolution and variability (spatial and temporal), the AOD values are often within the representation error and measurement uncertainties (refer to section 4.4 and 4.5). For SSA, underestimation is most pronounced at shorter wavelengths (<500nm), with absolute bias decreasing at longer wavelengths, as will be further discussed in the next section.

Since column-averaged SSA at 440 nm typically ranges between 0.75–1.00 under ambient conditions based on observations from both AERONET and SPEXone, a negative bias from the EAC4 simulations indicates that satellite-detected aerosol is less absorbing compared to model assumptions. Therefore, the simulated absorption AOD (AAOD) is overestimated. Overestimated total AOD may also be due to excess modelled aerosol burdens, but the mismatch in SSA suggests compositional and/or optical parameterization also contribute to error.

4.3.2 SSA experiments

Given the previous results showing the high uncertainty associated with SSA, this section focuses on comparison of SPEXone land retrievals with modelled SSA.

4.3.2.1 Sensitivity experiments

For each of the six experiments with a focus on SSA listed in Table 2, Figure 4-9 shows maps of the global bias with SPEXone observations. The same comparisons during the same period has also been made with AERONET stations, with the results available in Appendix E. In the SSA experiments, we made a conscious choice to combine hydrophilic and hydrophobic OM together as a single specie for simplification in the uncertainty estimation. For the BC experiments, doubling SSA reduces biases similar as shifting 25% of BC to OM, which has higher SSA. Slightly increasing the SSA of OM by 0.2 (not shown) and 0.4 raises SSA overall more effectively than the BC experiments do, since in EAC4 data, OM is the main contributor globally to modelled AOD (see for example Figure A-1) but also SSA (not shown). Combining BC and OM adjustments mostly corrects underestimations, except in the Sahara, Taklamakan, and Australian deserts. Using the Dubovik et al., 2002 dust description results in a lower absolute mean bias for SSA. Combining these experiments shows a reduced absolute bias. These experiments do not clearly suggest that applying such changes in the IFS model would be immediately beneficial. Instead, increasing the SSA sensitivity associated with the individual aerosol species might have a stronger impact.

Figure 4-10 shows the spectral error from each of the experiments. The originally modelled SSA consistently underestimated observed SSA by approximately 0.06; observed values typically fall within the 0.75 to 1.00 range, with the largest underestimation noted in lower UV spectrum. The overall SSA correlation is quite low with values <0.3 for around 1000nm, and about 0.1 around 500nm, while AOD (Figure D-2) has correlation of 0.8 for short wavelength and drop to just above 0.6 for longer wavelengths. Perturbing the SSA (by doubling black carbon SSA and increasing OM SSA by 0.004 with a maximum of 1.0) reduced the bias across wavelengths to less than 0.04. Further, switching the dust optical description from Woodward to Dubovik minimized the bias further, bringing it within ±0.01, and also resulted in a decreased root-mean-square-error (RMSE) compared to the original model, particularly at lower wavelengths. The Dubovik dust scheme produced the largest differences at wavelengths below 550 nm.

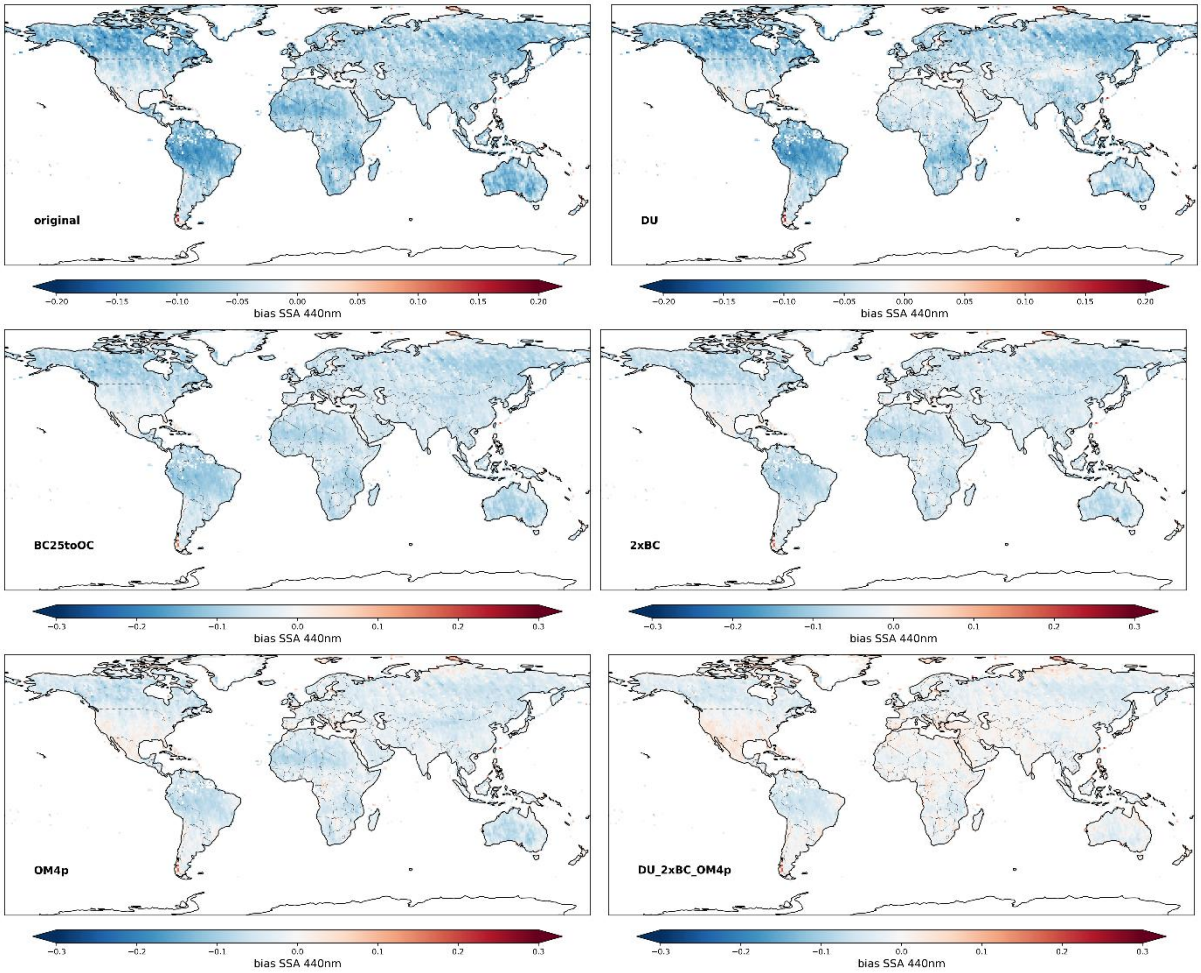

Figure 4-9 - Experiments on vertical column of SSA (from left to right and top to bottom): (1) original, (2) Dubovik scheme, (3) doubling SSA of BC, (4) moving 25% of BC to OM, (5) add 0.4% SSA of OM, and (6) Dubovik dust optical properties combining with (2),(4), and (5).

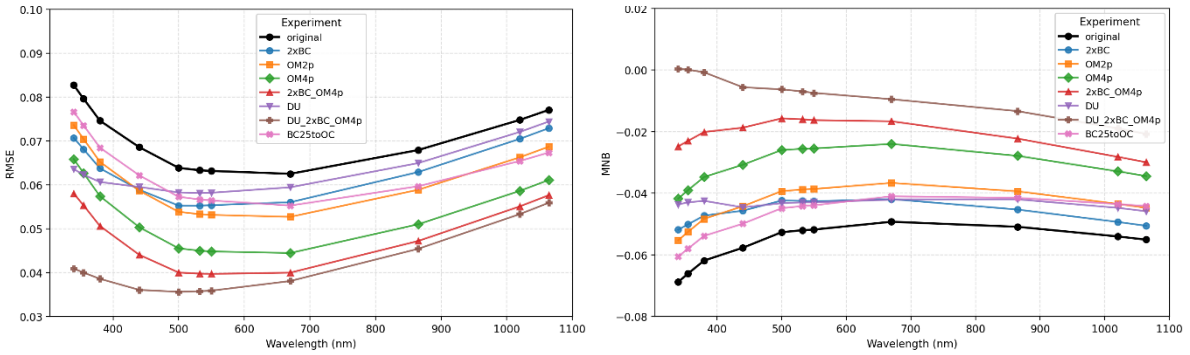

Figure 4-10 - SSA RMSE and Mean Normalised Bias (MNB) over spectra of 1x1 degree gridded monthly averaged of modelled error comparing to SPEXone.

4.3.2.2 Regional evaluation

Based on AOD observations from SPEXone, four regions with high AOD and good temporal coverage are selected for detailed analysis of experiments on SSA representation.

Congo Basin

Figure 4-11 shows the results of three of the experiments for the region of Congo/Central Africa, which is one of the largest global sources of biomass burning. The results of an experiment are compared against the original default setup. Originally, the model estimates SSA between 0.8 and 0.9, whereas the SPEXone SSA lies between 0.85 and 1.00. Clearly, the model underestimates SSA in this region, consistent with previous results.

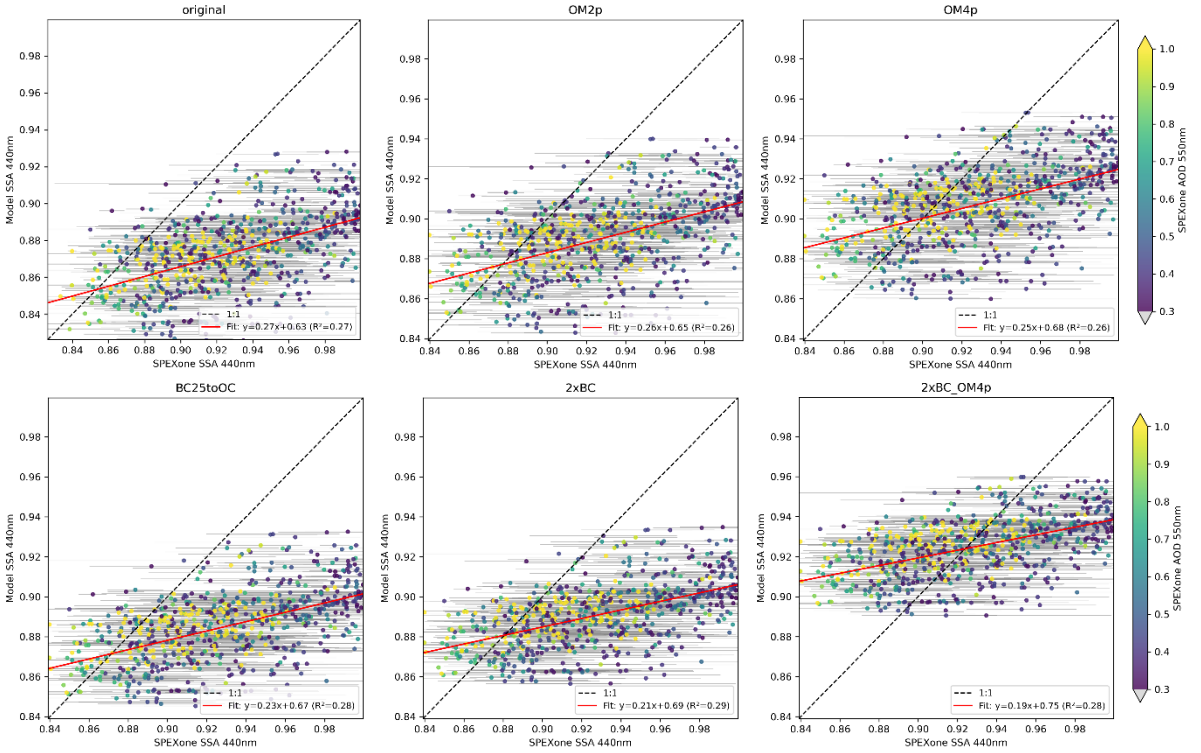

Figure 4-11 - The results from the SSA experiments in the Congo region at 440nm: 1) default setup 2) OM plus 0.2% SSA 3) OM plus 0.4% SSA 4) 25% BC mass to OC (5) double Black Carbon SSA (6) combining 3 and 5. Each point is 1x1 degree monthly re-gridded SPEXone observation median with bar representing standard deviation with collocated modelled SSA. Plotted data have filtered with AOD above 0.3 at 550nm, and colour is SPEXone AOD at 550nm.

The observed SSA in the Congo basin indicates that high AOD (colour of the scatter plot) is often associated with low SSA, and vice versa. Since the Congo basin is often associated with active biomass burning also including agriculture and domestic demand, the aerosol emitted from dense smoke is more absorbing and contains a high amount of black carbon from incomplete burning. The model is able to capture this trend correctly despite SSA being overall lower than SPEXone.

Increasing the SSA of all OM significantly decreases the bias between modelled and observed SSA. Doubling BC (2xBC) SSA drastically increases SSA wherever BC is present, and it provides an insight on the sensitivity of the BC/OM ratio. For another experiment (BC25toOC) which aims to change the OC/BC ratio directly, it shows a similar effect as 2xBC but a slightly smaller impact on SSA. Both BC experiments decrease the overall bias while increasing the slope of the linear fit; the overestimation suggests that aerosol mixtures with high AOD could be more absorbing when BC is present. Combining these two approaches, the modelled SSA range agrees better with the observations. Note that 2xBC_OM4p experiment still has a

narrow range of 0.89 to 0.96 and produces an overestimation of SSA during high AOD observations.

Canadian peatland

The peatland burning on high latitudes is often associated with emission of brown carbon which leads to a highly reflective smoke compared to other biomass burning. Figure 4-12 shows modelled and observed AOD data in the peatland area in Canada with observed AOD>0.1. Based on the observations, SSA is mostly around and above 0.95 during high AOD moments. In contrast, the model considers these aerosols as being highly absorbing with SSA between 0.7 to 0.85. Both doubling SSA of BC and +0.2% or 0.4% OM increases overall modelled SSA. During high AOD (>0.3) events, the observations are consistently showing column SSA around 0.95 +-0.05. Filtering on AOD value is important here, as the SPEXone SSA has larger errors for low AOD (Fu et al., 2025). Experiments with perturbed OM and BC did not show significantly different results during these high AOD and reflective events. These experiments did not improve the linear regression fit between model and observations, and is therefore possibly the result of the underlying modelling assumptions (most likely the assumed optical properties of organic matter).

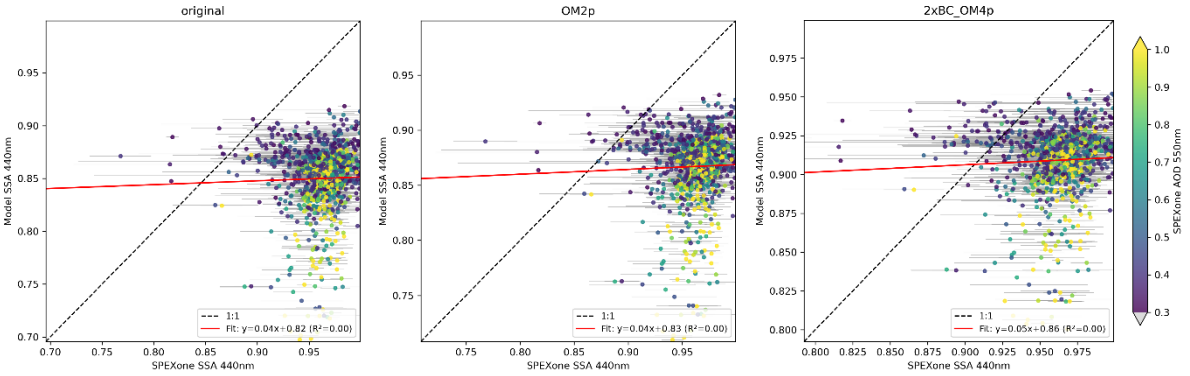

Figure 4-12 - The results from selected SSA experiments at 440nm in the region of peatland in Canada: 1) default setup; 2) OM add 0.4% SSA; 3) double BC combines with OM add 0.4% SSA. Each point is 1x1 degree monthly re-gridded SPEXone observation median with the error bar representing standard deviation with collocated modelled SSA. Plotted data has been filtered with AOD at 550 nm above 0.3. The colour indicates SPEXone AOD at 550nm.

Sahara

Figure 4-13 illustrates observed desert dust dominated SSA in the Sahara. The Dubovik scheme yields less variable SSA values (mostly 0.92–0.95), the composite scheme (Figure F-1, Appendix F) shows a similar range but matches slightly worse with SPEXone than Dubovik, while with Woodward's the modelled SSA range is 0.83–0.95. The SPEXone retrieved SSA ranges from 0.83 to 1.00. None of the three schemes captures highly reflective events, revealing similar limitations noted for OM and biomass burning. However, Dubovik aligns better with observations during high AOD periods, when SSA tends to be higher; by contrast, Woodward typically associates high AOD with SSA below 0.92. Additionally, switching the dust scheme does not affect total AOD significantly (Figure F-2, Appendix F), with Woodward (original) showing the best agreement (R^2 = 0.50), followed by Dubovik (R^2 = 0.48) and Composite (R^2 = 0.45).

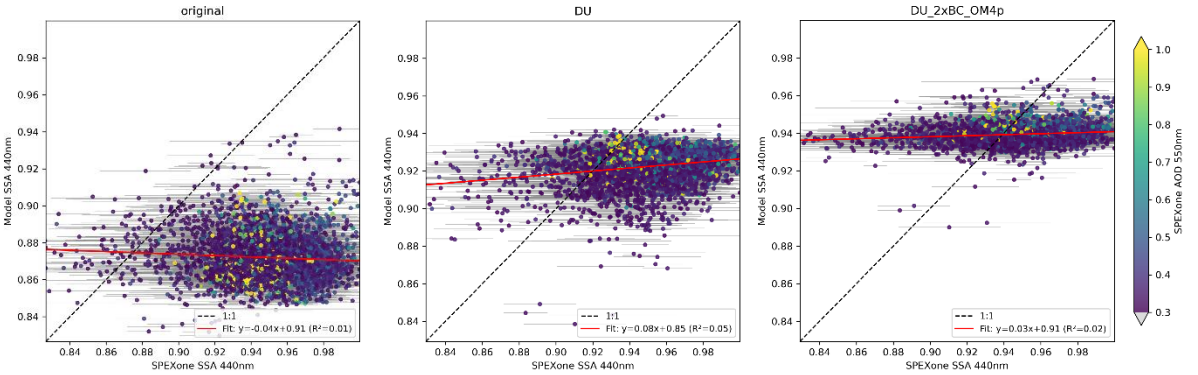

Figure 4-13 - The results from selected SSA experiments at 440nm in the region of the Sahara: 1) default setup; 2) using Dubovik instead of Woodward dust; 3) OM add 0.4% SSA and double Black Carbon SSA and Dubovik dust. Each point is 1x1 degree monthly re-gridded SPEXone observation median with the error bars representing standard deviation with collocated modelled SSA. Plotted data has been filtered with AOD at 550 nm above 0.3. Colours indicate the SPEXone AOD at 550nm.

Northeast India

In Northeast India, particulate matter pollution is a complex mixture from fossil fuel emission, to biomass burning, and seasonal dust intrusion from Indian desert. Similar to the cases above, the model underestimates SSA and systematically fails to capture any case of SSA above 0.95 (Figure 4-14). The observation during high AODs (>0.5, for example) no longer occurs with low SSA. Contrary, lower AOD instances generally coincide with low SSA and high AOD instances model coincide with high SSA. In the observations, SSA varies in both cases between 0.88 to 1. Compared to the Congo basin, Indian air pollution events contain less black carbon and possibly results from a mixture of source that has less incomplete burning during high AOD events than central Africa.

Doubling BC SSA has reduced the bias but also increased the modelled SSA during high SSA days. Increasing the SSA of OM reduces the bias of SSA more effectively than changing the SSA of BC. We also found that dust could attribute to the errors in this region, where using the Dubovik dust scheme increases SSA but also results in a narrower range of SSA. Meanwhile, Dubovik reduces outliers when the model significantly underestimates the SSA.

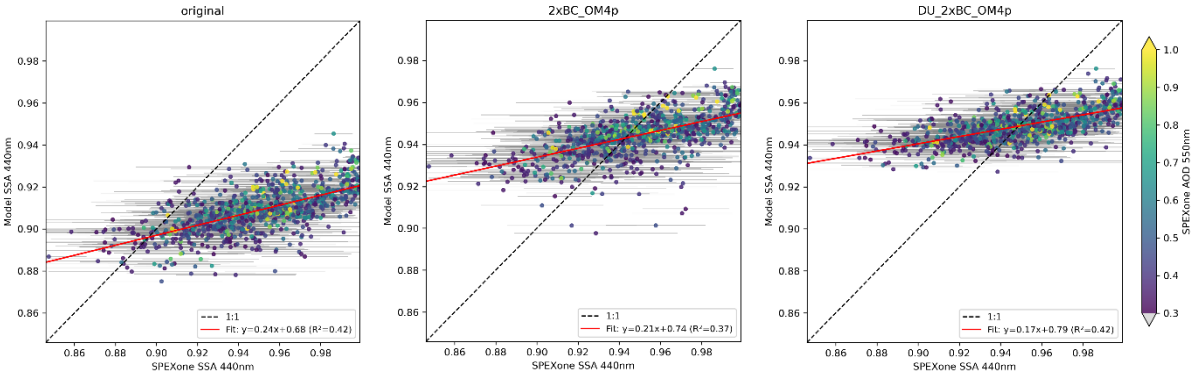

Figure 4-14 - The results from selected SSA experiments at 440nm in the region of northeastern India: 1) default setup; 2) OM add 0.4% SSA and double Black Carbon SSA; 3) combining 2) with dust based on Dubovik scheme. Each point is 1x1 degree monthly re-gridded SPEXone observation median with error bars representing standard deviation with collocated modelled SSA. Plotted data have filtered with AOD at 550 nm above 0.1. Colours represent SPEXone AOD at 550 nm.

Summary of monthly SSA sensitivity

With all the sensitivity experiments on SSA, Figure 4-15 shows the monthly mean SSA from model and SPEXone retrievals. Although these optical perturbations without changing refractive index and other physical processes would not affect variabilities (with the exception of changing the dust scheme), the new set of DU_2xBC_OM4p experiments are able to capture most of monthly average SSA values using SPEXone observations as reference. However, modelling the brown carbon dominated areas or the white smoke from peatland burning in Canada remains challenging. Without changing local mixtures of aerosols and their optical representation, it would be difficult to capture the biomass burning season SSA using assimilation.

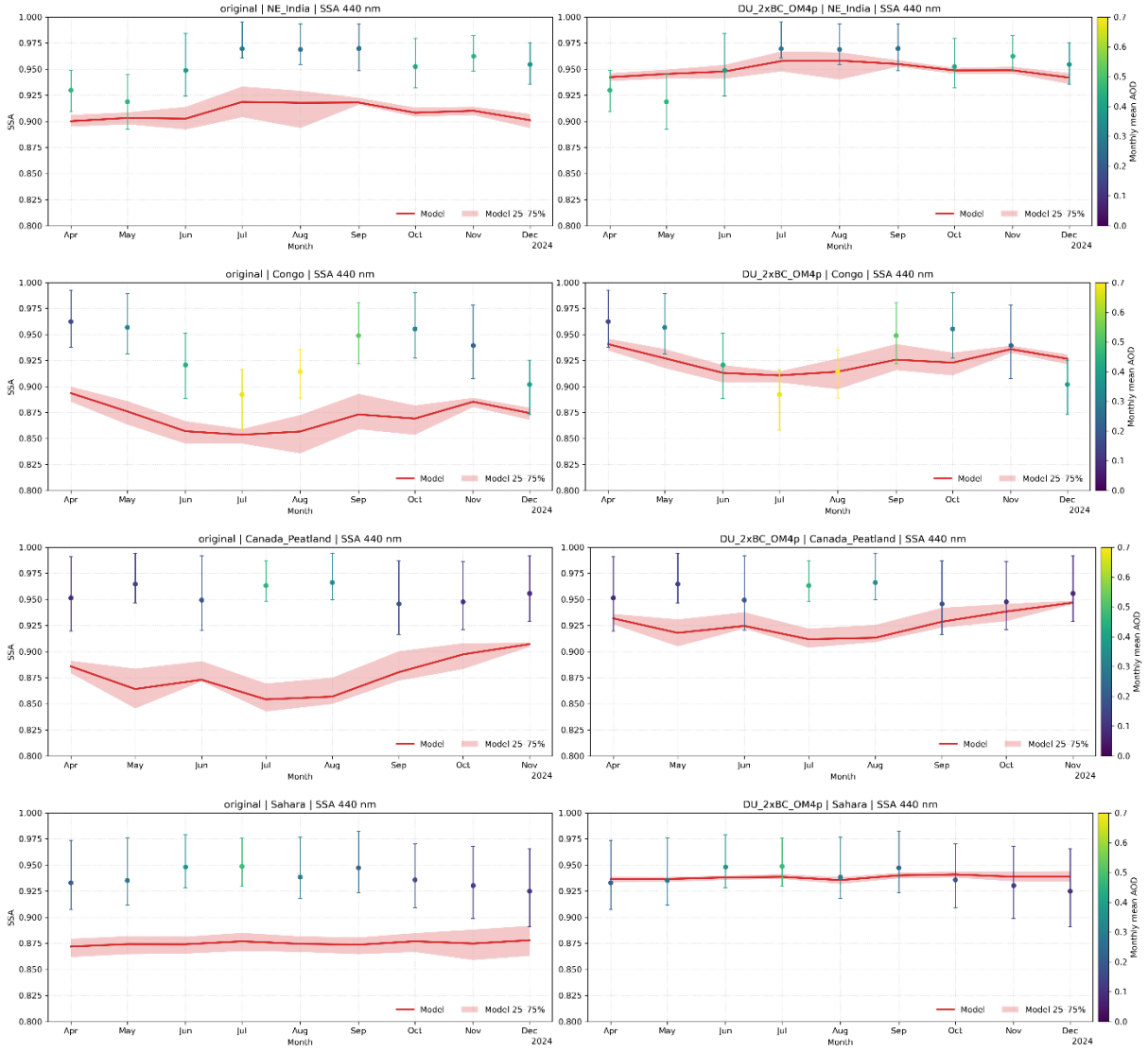

Figure 4-15 monthly modelled mean SSA in red comparing to SPEXone mean SSA in points with the colour of monthly mean SPEXone mean AOD at 550nm. The errors indicate 25 to 75 percentile.

In summary, SPEXone-retrieved SSA values are frequently very high (approximately 1.0), yet the model does not produce such elevated SSA values, which are consistent with AERONET observation in 2023. The analysis of SSA globally demonstrates that modifying black carbon and organic matter properties reduce overall model bias and error. Switching to the Dubovik dust optical scheme especially improves the results in dusty regions like the Sahara for short wavelengths. This adjustment also leads to a closer alignment with SPEXone observations, particularly during high AOD periods and at lower wavelengths, with the remaining bias largely

confined within ±0.02. However, some discrepancies persist, notably the model's inability to replicate the highest observed SSA values and its limited capacity to capture the full variability and correlation. It underlines the assumption that the imaginary part of the refractive index does not fully reflect the correct aerosol mixture state and hygroscopic growth. These assumptions regarding aerosol optics will be discussed further in subsequent sections. Given the limited agreement between optical setup of SSA in the model version used in the CAMS Reanalysis, it will be worthwhile to assess the SSA performance also in a more recent model version, considering the range of improvements made since then. Indeed, use of SSA for assimilation directly requires such in the current forward modelling parameterization. Hence the following section on sensitivity and variability of aerosol concentrations will focus on AOD only.

4.4 Sensitivities and variability of aerosol concentrations

An import preparation for assimilation is the evaluation of correlation length scales. Spatial and temporal correlation lengths indicate how far in distance and time an observation can affect the model state. An appropriate correlation length scale can reduce overfitting, which also is a key component for background error covariance (Section 5).

4.4.1 Temporal correlation & observation

Temporal correlation length, determined by when the autocorrelation value falls below 1/e, varies for all grid cells globally as seen in Figure 4-16. Outside the Arctic regions, areas like the Congo and Amazon basins in tropic exhibit month-long correlation lengths (~720 hrs), suggesting persistent, slow processes likely tied to consistent biomass burning. The plumes from these regions on land and their downwind area persist over long periods. Assimilating observations in these regions means that values persist longer, making instruments with infrequent revisits, such as SPEXone, still useful. In contrast, ocean and deserts shows low correlation lengths, as atmospheric storms, meteorological and ocean circulation dominate the aerosol advection and emission, shows low correlation lengths. For instance, the Southern Ocean and the North Atlantic have correlation lengths less than a day, indicating aerosols are dominated by short-lived species or rapidly changing emissions due to variable wind. In between these two extremes, mostly of industrialized regions like India and China has correlation length of several days to a week.

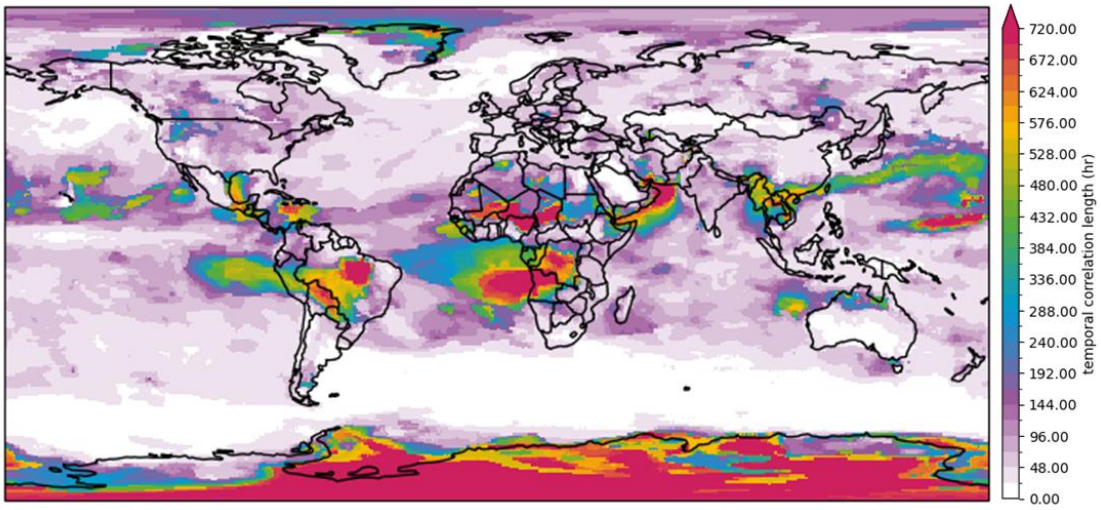

Figure 4-16 - Temporal correlation length scale in hours calculated in the same period of SPEXone observations April to December 2024.

4.4.2 Local spatial correlation lengths in the IFS model

Using the IFS model data we can determine the spatial correlation length using the following method. For each location a neighbourhood of 20x20 model grid cells is selected. For all of these points the correlation with respect to the point of interest is calculated. The correlation at the point of interest is 1 and drops of with increasing distance. If we fit the correlation as function of distance with a gaussian function we can determine the spatial correlation length. Graphically the method is explained in Figure 4-17. This method can be applied to all grid cells which results in a spatially varying spatial correlation length. This correlation length indicates how representative the AOD (or another metric of interest) at a specific location is for AODs in its vicinity.

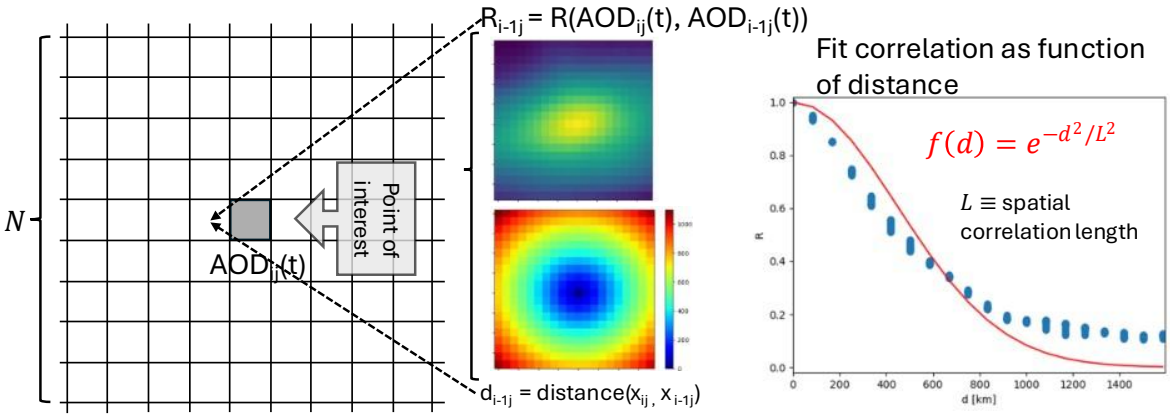

Figure 4-17 Graphic depiction of the method to determine the spatial correlation length.

The resultant correlation length for the AOD at 550nm is shown in Figure 4-18 The annual spatial correlation The average correlation length is about 700km with a standard deviation of about 150km. This figure shows that near the equator correlation lengths are larger and terrestrial AODs on average have a lower correlation length.

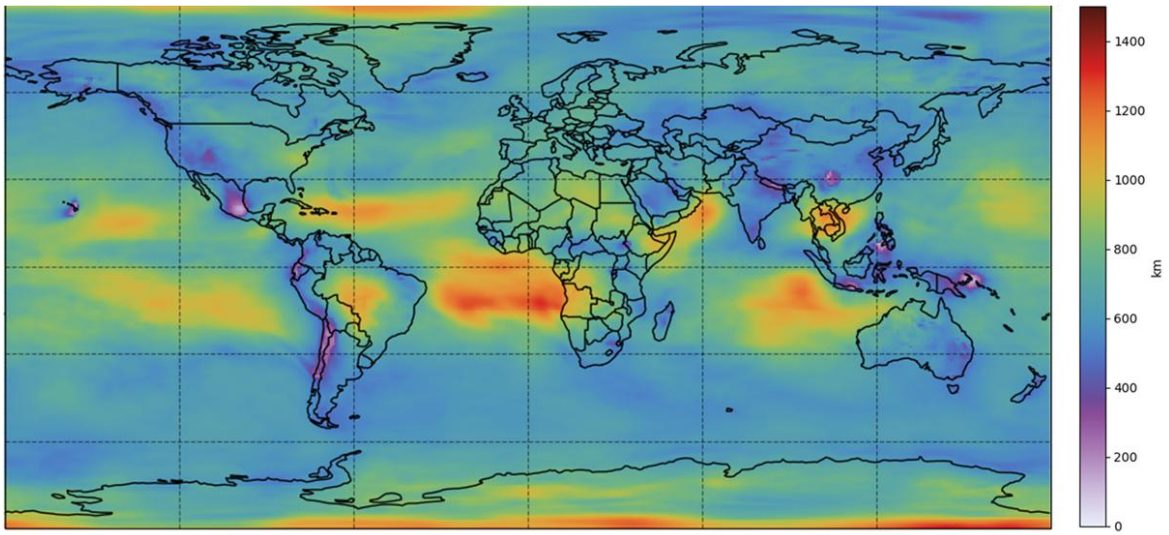

Figure 4-18 The annual spatial correlation length in kilometre using modelled total AOD at 550nm

4.5 Maximum Likelihood Estimation on Uncertainties

4.5.1 AOD simulation and assimilation

In the IFS model, for each aerosol specie, the size and affinity towards water are for each aerosol type modelled separately in the optical routine. Therefore, they can be considered as all individual species with their own optical description[3]. With this approach, AOD can be presented as follows:

$$AOD_{\lambda} = \sum_{z} \sum_{s} MMR_{s,z} \; MEC_{\lambda,s,z} \; dm_{z} \qquad \text{Eq. 1}$$

In here, s refers to the aerosol specie, λ to the wavelength, and *z* to the model layer. The model states consist of 3D mass-mixing-ratios (*MMR)* fields for each time stamp that can be integrated to a total column using the air mass dm_z of the layers; the mass-extinction-coefficient $MEC_{\lambda,s,z}$ defines the optical extinction per wavelength, species, and layer-depended relative humidity.

The primary goal of assimilating AOD observations from for example satellites is to improve the simulated mass mixing ratios of the aerosol components. For this it is necessary to first define the uncertainty of the MMR values, to know to which extent they might be modified by an assimilation procedure. Not only the uncertainty of individual MMR simulations should be quantified, but also how these are correlated with uncertainties of MMR values in other species and in other grid cells at other moments. This uncertainty description is usually parameterized using standard deviations, length scales for spatial and temporal correlation, and assumptions about correlations between different aerosol species. If these parameters are chosen well, the uncertainty in MMR's implies an uncertainty in simulated AOD such that AOD observations are within the simulated uncertainty range. Suitable values for the uncertainty parameters could be obtained using *Maximum Likelihood Estimation (MLE),* following for example (Henne et al., 2016). With MLE, the most likely value of uncertainty parameters could be chosen that could best explain the observed differences between (uncertain) observations and (also uncertain) simulations.

The current AOD assimilation in IFS applies corrections to the total aerosol mass, keeping the distribution over species the same. This is suitable in case AOD from only a single wavelength is assimilated, as no further information on individual species is available. However, with the multi-wavelength data from for example SPEXone it becomes feasible to distinguish multiple species or groups of species in the assimilation. We will use MLE to obtain insight in the amount of uncertainty that is needed to explain the differences between simulations and observations when organic matter aerosols are considered distinct from the other aerosols. The MLE is applied per grid cell to obtain suitable uncertainties for individual total column aerosol masses; although the technique could be used to obtain correlation length scales, this is left for future.

4.5.2 Maximum Likelihood Estimation

To apply MLE, we first define *x* to be a state vector that consists of one or more summed aerosol masses in grid cell. If only the total aerosol is considered to be uncertain, then *x* has just one element. The following relation is defined between the state vector *x* and the observation vector *y*, which is here the SPEXone observed AOD at multiple wavelengths:

$$y = H(c)\, x + \mathrm{v} \qquad \text{Eq. 2}$$

Here, v represents the error between the simulations and observations, which includes representation error, instrument error, and retrieval error; it is assumed to be a sample from a

[3] https://www.cameo-project.eu/sites/default/files/2024-08/CAMEO-D1-6-V1.0.pdf

multivariate Gaussian distribution with zero mean and covariance *R* The observation operator $H(c)$ is implemented as follows:

$$H(c)=A\,I(c)\,G \qquad \text{Eq. 3}$$

In here, G is distributes the summed aerosol masses in x over the individual aerosol species; in case only total mass is considered, then *G* is just a column with the fractions of the total mass per species. Diagonal matrix $I(c)$ has the aerosol loads of all species as the diagonal elements. Operator A simulates the optical properties of the aerosol composition. In this study, these are obtained from the OOPP observation operator output, based on the mass extinction coefficient from the optical look-up table.

For the state vector *x* an uncertainty is defined using parameters α:

$$x \sim N(x_b, P_\alpha)$$

The parameters in α typically contain the standard deviations of the considered aerosol sums, and correlations between the sums (if defined). Following estimation theory, the best parameters in α are those that maximise the likelihood of the observations:

$$L(y|x) \propto (y\text{-}Hx)\,\Sigma^{-1}(y\text{-}Hx)^T + log|\Sigma| \qquad \text{Eq. 4}$$

where Σ = $H\,P_\alpha H^\mathsf{T}$ + R is the covariance of the error between observations and simulations. The operations on Σ can be implemented using Cholesky decomposition.

4.5.3 Split in aerosol composition: organic matter vs rest

The existing assimilation often uses AOD at one wavelength (e.g. 550nm) to explain fully correlated aerosol fields where all aerosols are scaled up or down simultaneously (Garrigues et al., 2023). As seen in previous sections, the simulated optical properties are most sensitive to organic matter (OM). As first step in introducing uncertainty in the aerosol composition, we therefore suggest to split the aerosols into 2 groups: one holding OM (hydrophilic and hydrophobic), and one for the rest. Following the notations introduced above, the covariance matrix is thus a 2x2 matrix. We assume no correlation between the groups, and the covariance matrix is thus parameterized by just 2 standard deviations:

$$P_\alpha = \begin{pmatrix} \sigma_{rest} & 0 \\ 0 & \sigma_{om} \end{pmatrix} \qquad \text{Eq. 5}$$

For the observations we chose to use multi wavelength AOD at 340, 355, 380, 440, 500, 532, 550, 670, 865, 1020, 1064nm from SPEXone. The sensitivity experiments in previous sections showed that current simulation of SSA is limited, and therefore these observations are not considered here. The Maximum Likelihood Estimation is performed at gridded fields at 1°x1° with the default IFS setup (with Woodward dust). Since SPEXone has an overpass roughly about once every month globally, both observations and simulations are also averaged to a monthly frequency. For the observation representation error covariance *R* in the MLE method, the errors are assumed to be uncorrelated (*R* diagonal) with standard deviations set based on the spread of the observations within a month, with a minimum of 0.02 following the reported instrumental error.

As illustration, Figure 4-19 shows timeseries of AOD at 440 nm from April to December at 4 selected locations (see also the marks on the maps in Figure 4-20). Each panel shows the monthly median observations in red, with an error bar to indicate the value range within the month. The black line shows the default simulation. For each location the with MLE optimized uncertainties of organic matter and remaining aerosol are used to indicate the 1-σ simulation range: the green area if only organic matter is considered uncertain, the purple area if only the rest is considered uncertain, and the grey area if both are considered. The top panel shows the timeseries for an arid location in Peru, which is downwind from regions where biomass burning is important. Uncertainties in organic matter could therefore explain the observations

rather well. For the point located in Greece, high uncertainties in OM are associated with the fire season in Mediterranean; outside of the fire season the uncertainties are due to other aerosols. At the location of United Arab Emirates, where aerosols stem from a mixed of desert and urban settlements, the time series show that during spring and summer uncertainties in organic matter emission could explain the differences with observations, while for the other months not much uncertainty is needed anymore. It also gives an insight into the origin of the long temporal correlation for this location as shown in Figure 4-16, as the difference with observations is very consistent over time. For the location in the Sahara, modelled OM sensitivity shows almost no impact on the timeseries of AOD. Since the location is dominated by dust, the uncertainty was correctly attributed to the rest of aerosol instead of OM. Moreover, the underestimation of annual AOD in Figure 4-8 can be explained by the large variability of observation shown in the timeseries.

In the selected time series it can be seen that in general the model simulations overestimate the observed AOD at 440nm, in particular when organic matter is the dominant aerosol. This suggests that either the mass extinction coefficient at 440nm for organic matter is too high, or that the burden of organic matter in the simulations is too high.

Figure 4-20 shows global maps of the standard deviations obtained with the MLE for the organic matter part (top) and the rest of the aerosols (bottom). Based on the geographical distribution, the *rest* aerosol has higher uncertainty in the locations where dust aerosol is dominant, and over locations over land that are dominated by sea salt. Overall, the uncertainty assigned to organic matter is higher than the uncertainty assigned to the *rest* aerosol. Thus, to be able to explain the simulation bias with multi-wavelength AOD observations, it is especially necessary to consider the organic matter load as uncertain.

Note that organic matter is spectrally more sensitive to wavelengths in UV and Visible range, while dust (based on Woodward scheme optical settings) as part of the *rest* aerosols is more equally sensitive to all wavelengths. For long wavelengths near 1000 nm, the uncertainties in *rest* aerosols therefore explains a larger portion of the difference with observations.

Overall, the results indicate that adjusting organic matter in assimilation separately from the other species could be a first promising step when using multiple wavelengths in the assimilation.

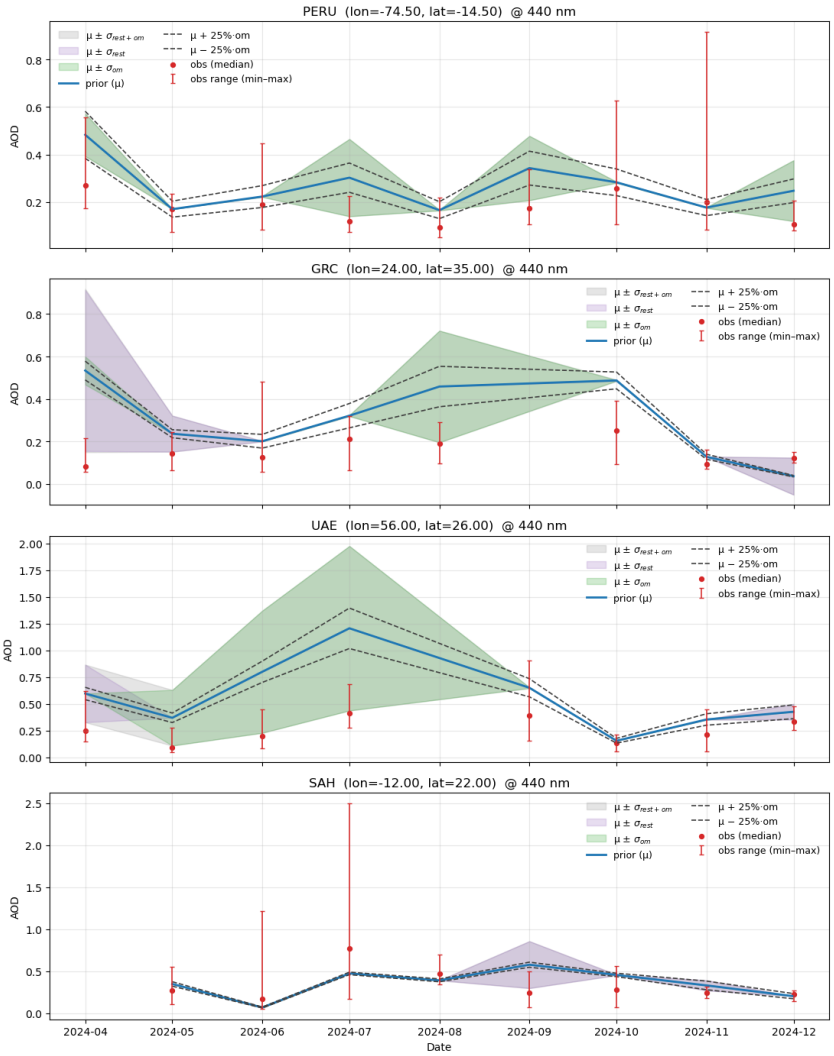

Figure 4-19 - Observed and simulated AOD at 440 nm including uncertainties for locations in Peru, Greece (GRC), U.A.E. (UAE), and west of Sahara (SAH). The dashed line indicated the 25% sensitivity of AOD_{om} at 440nm. Shaded areas show the 1-std.dev. range given the uncertainties in organic matter (green) and other aerosols (purple) obtained using the Maximum Likelihood Estimation. The observation (SPEXone) uncertainties (minimum to maximum) is shown as the red bar with median of observation.

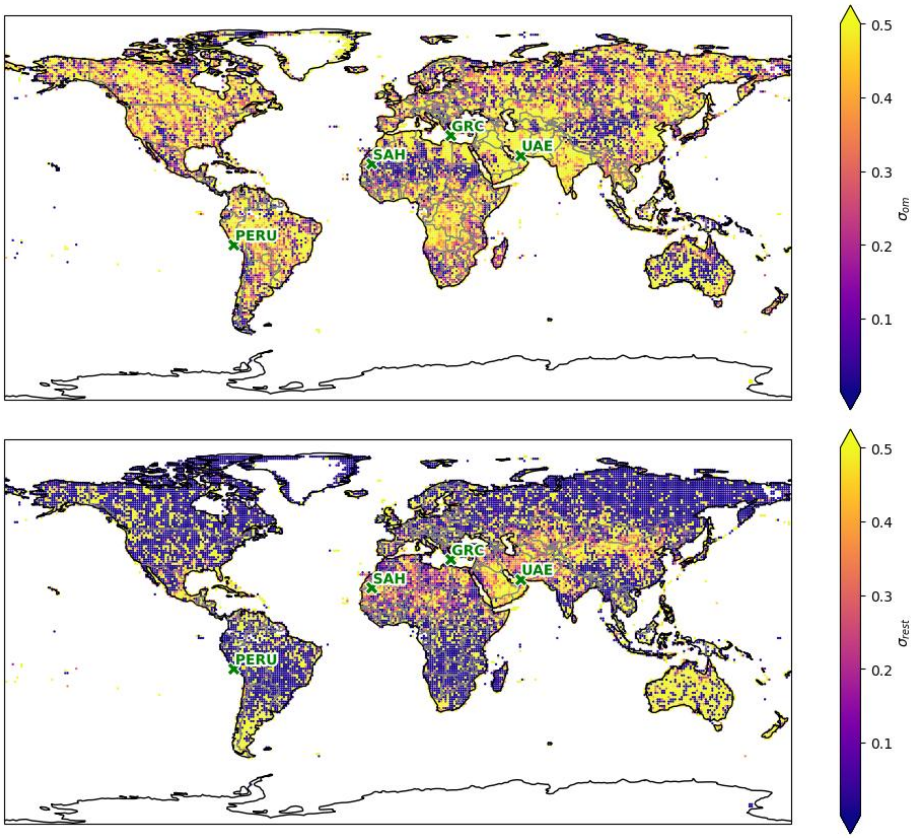

Figure 4-20 - Averaged 2024 April-December monthly mean standard deviation of Organic Matter (σ_{om}) and rest (σ_{rest}) as obtained with Maximum Likelihood Estimation. The 4 locations chosen for the timeseries plots are marked in green.

5 Discussion and Recommendation

From the experiments described in this report, the following overall conclusions and recommendations have been drawn.

5.1 Importance of additional optical diagnostic variables

Compared to the first version, the latest OOPP supports non-AOD variables such as SSA and ASY that could be used for validation of optical properties simulated by IFS. The extension to other variables is important since AOD is a bulk metric that does not provide detailed information on the aerosol composition and the vertical distribution. Taking into account spectral information in both AOD and SSA gives access to additional information, for example on vertical profile based on extinction and backscatter and on dust load based on depolarization ratio.

5.2 Validation with new instruments

Capabilities were developed in OOPP to compare with measurement data (e.g., satellite and AERONET AOD data, but also other measured quantities like backscatter and extinction profiles). The SPEXone satellite instrument provides global coverage for SSA which is a significant extension compared to the limited spatial and temporal coverage of SSA observations available from AERONET. OOPP could therefore quickly compare and validate different optical setups for new developments to compare with observations, and subsequently improve the IFS model and its reanalysis capabilities.

5.3 Evaluation of AOD and SSA

The analysis of AOD results shows an overall global overestimation by IFS simulations in the CAMS global Reanalysis (EAC4). Similar to Xian et al. (2024), a comparison study across multiple reanalysis datasets, we found high uncertainty associated with biomass burning, with a positive bias, and an underestimation of AOD in regions with high dust loads. In addition, the CAMS reanalysis data failed to capture SSA variability. However, it should be noted that the optical setup has been updated in more recent cycles of IFS-AER, such as dust and organic matter optical schemes. The SPEXone satellite instrument provides global coverage for SSA to evaluate model uncertainties, and is a significant extension of the limited spatial and temporal coverage of SSA observations available from AERONET. Lastly, OOPP can quickly compare and validate different optical setups for new developments to compare with observations.

In the analysis of both AOD and SSA, we found high uncertainty and high sensitivity associated with organic matter (OM), especially hydrophilic OM. Given that the model version evaluated here treats this large component as a single bulk group, such an assumption may overlook the variation in water uptake among different organic aerosol types. Comparisons with AERONET observations indicate that the hygroscopicity of wet organic matter (WOM) is overestimated in the model version used for the CAMS reanalysis when it is represented as a whole. Figure A-1 shows the contribution per specie to AOD in AERONET sites and the OM contribution over the globe according to the model output. Given the large contribution of the OM mixture in the IFS model in general, especially in the biomass burning region in forested areas, the optical description of OM becomes critical for modelling the optical diagnostics. The OOPP will soon be updated to support also the optical codes and lookup tables used for recent IFS versions, which will be used to evaluate the progress made on this.

5.4 Sensitivity for dust optical properties

For the dust scheme, Woodward assumes an imaginary refractive index of 0.0057, while Dubovik et al., 2006 uses 0.0022 derived from AERONET measurements at 500nm, and the composite scheme lies somewhere between Woodward and Dubovik. From the perspective of AOD, the selected scheme matters very little. However, in the IFS system, the aerosol direct

effect also changes the atmospheric heating rate and meteorology. Therefore, Bozzo et al., (2017) has already made comparison for the Dubovik and Woodward dust optical properties, which aligned with our results. Woodward is significantly more absorbing, as indicated by its refractive index in the shortwave range (thus lower SSA). The reasoning for choosing Woodward is that IFS shows a negative bias in temperature in dusty regions, which would be amplified with the Dubovik scheme. However, in this study, we found that the Dubovik scheme provides a significantly better SSA than Woodward compared to the observed SSA in SPEXone. Hence, the temperature bias might not be caused by the SSA assumption; instead, it should be attributed to underlying meteorological processes or to the radiative transfer calculation. For example, we found that ASY has been underestimated by the model at AERONET sites (Figure 4-3), indicating greater backward scattering and thereby enhancing the cooling effect. Moreover, dust composition can also contribute to the temporal and spatial variability of SSA which are not captured well by all three schemes. It is known that the presence of iron changes the refractive indices, and is affecting SSA, which was measured varying between 0.99 and 0.86 in different arid regions in Eurasia and Africa (Moosmüller et al., 2012).

5.5 Optical properties of black carbon

There are debates on whether atmospheric models have overestimated the climate-positive forcing associated with black carbon (BC). The imaginary part of the refractive index directly reflects aerosol absorption, which affects SSA. This study demonstrated that doubling the SSA of BC reduces the absolute bias w.r.t. SPEXone. One could also argue that there is too much black carbon in the column. However, the aerosol mixing assumption in IFS treats BC as pure soot, externally mixed, and OM (OPAC Mixture; Hess et al., 1998) as a black carbon mixture. In LUTs, pure BC (OPAC) would have an SSA of 0.2-0.3 between 350 and 600nm. Therefore, the model assumes some BC are externally mixed, but with OM, BC has been coated with other organics. Recent studies (Romshoo et al., 2024; Wang et al., 2023; Zeng et al., 2024) have shown that various parameterizations on heterogeneous mixing state and morphology of BC can improve the modelled light absorption over existing external mixing and core-shell mixing assumptions.

5.6 Variability in SSA

Based on the comparison of SSA and AOD against AERONET and SPEXone observations, it is recommended to use the Dubovik scheme for the dust SSA. For biomass burning regions the IFS model consistently underestimates the SSA. Perturbation experiments show that increasing OM and BC can decrease the SSA bias. Doubling the BC SSA could also decrease the model bias, but a similar effect can be achieved by modifying the OM mixture assumption, or by introducing a new OM/BC mixing-state parameterisation. In addition, current modelling approaches cannot capture the variability of SSA over peatland burning regions in Canada that is observed by SPEXone. This is likely caused by the use of a generic model without a detailed BC/OM representation for brown carbon, or by biases in the fire emissions.

5.7 Guidelines for assimilation

5.7.1 Separate assimilation of organic matter

Our analysis indicates that variations in the size bins and optical descriptions of naturally emitted dust have a negligible effect on the global bias in AOD compared to observations. In contrast, OM emerges as the dominant contributor to both global AOD values and their associated uncertainties. Therefore, if operational constraints limit the number of assimilated species, the greatest impact would likely be achieved by assimilating OM separately instead of assuming fully correlated aerosol species.

To show the potential for separate assimilation of OM from the rest of the aerosols, we used a maximum likelihood estimation (MLE) approach for the uncertainty estimation. In this simplified approach, the uncertainty in OM was assumed to be uncorrelated from the uncertainty in the remaining species. Note that although this allows the aerosol masses of OM

and the remaining species to be varied independent from each other, a significant correlation might still be present, as shown in Figure A-2 (Appendix A). These The correlation between aerosols is important, but yet often overlooked or simplified in assimilations. Yet this targeted approach with a focus on OM still yields substantial gains in aerosol representation compared to assuming a fully correlated aerosol composition.

5.7.2 Assimilation of multiple wavelengths

The experiments performed in this study illustrated the wavelength dependency of IFS simulations. It is therefore recommend to focus on assimilation of multiple AOD wavelengths spanning the UV-vis-NIR spectrum rather than assimilating the Ångström Exponent to differentiate aerosol speciation. Using multiple wavelengths utilizes a broader wavelength range and therefore enhances the accuracy of aerosol characterisation.

5.7.3 Assimilation of SSA

Assimilating SSA offers a promising way to estimate and update this property in global models. Previous studies (Tsikerdekis et al., 2021; Yin et al., 2016) showed that SSA values are generally underestimated in models. Assimilation of AOD and aerosol column burden would not necessarily significantly improve SSA. Instead of keeping the underlying optical assumptions constant for SSA, we foresee a large gain by using assimilation to improve the accuracy of SSA assumptions per aerosol mixture regionally, rather than globally.

Nonetheless, SSA remains a valuable indicator of aerosol chemical speciation. To fully leverage SSA within data assimilation frameworks, it is crucial to refine the underlying assumptions, particularly those relating to the derivation of SSA from the imaginary component of the refractive index. Improving these assumptions will increase confidence in SSA for both aerosol modelling and meteorology forecasts.

5.8 Future developments

Continued development of OOPP, including its extension to handle additional wavelengths, smaller steps in water-uptake schemes, and new optical diagnostics, will further strengthen its role in supporting model validation and reanalysis efforts. Also, direct assimilation within OOPP with a focus on optical properties optimizations is conceivable. In particular, incorporating capabilities to compare with a wider array of measurement data—including satellite, AERONET, backscatter, extinction, and depolarisation profiles—will provide a more comprehensive evaluation of aerosol optical properties and foster improvements in both OOPP and the IFS model.

Looking ahead, these recommendations, will contribute to a more nuanced understanding of aerosol physical properties and processes, ultimately supporting the development of air quality, climate modelling, and reanalysis products in CAMS.

6 Conclusion

Aerosol optical properties play a crucial role in global atmospheric models, such as the Integrated Forecasting System (IFS), for meteorological and air quality forecasting, and for producing reanalysis data. This study explores key model biases, including the overestimation of Aerosol Optical Depth (AOD) associated with biomass-burning and the underestimation of Single Scattering Albedo (SSA) over land in the CAMS global reanalysis product (EAC4). To enable efficient, flexible evaluation, the standalone Offline-Optical-Post-Processor (OOPP) for the IFS model was used to evaluate modelled aerosol optical diagnostics against ground-based and satellite observations.

Multiple sensitivity experiments using OOPP reveal that organic matter (OM) is the dominant contributor to global AOD in modelled data, and its associated hygroscopic growth is influential and deserves further exploration. Tests with changes to dust mass partitioning and extinction coefficient show a limited impact on global AOD at selected AERONET locations. In contrast, adjustments to increase SSA of OM and black carbon (BC), along with the adoption of the Dubovik dust description, effectively reduce model bias in SSA while having minimal effect on AOD error. The sensitivity tests indicate that EAC4 generally overestimates the absorption of dust and biomass-burning aerosols due to slight overestimations of AOD and underestimations of SSA, particularly at short wavelengths in the UV-visible spectrum. Uncertainty estimation shows promising results for distinguishing OM from other aerosol types using AOD at multiple wavelengths from SPEXone. Therefore, we recommend testing assimilation using multi-wavelength AOD observations spanning the UV to NIR range, or at least consider assimilation of single-wavelength AOD in combination with Ångström exponent.

Acknowledgement

Partial computation of SPEXone data from PACE mission was performed on CryoCloud (NASA grants 80NSSC22K1877, 80NSSC23K0002, Snow 2023). Copilot was used in editing the texts.

Bibliography

Balkanski, Y., Schulz, M., Claquin, T., & Guibert, S. (2007). Reevaluation of Mineral aerosol radiative forcings suggests a better agreement with satellite and AERONET data. *Atmos. Chem. Phys.*

Bozzo, A., Remy, S., Benedetti, A., Flemming, J., Bechtold, P., Rodwell, M., & Morcrette, J.-J. (2017). *Implementation of a CAMS-based aerosol climatology in the IFS* (Vol. 801). European Centre for Medium-Range Weather Forecasts Reading, UK.

Di Biagio, C., Formenti, P., Balkanski, Y., Caponi, L., Cazaunau, M., Pangui, E., Journet, E., Nowak, S., Caquineau, S., Andreae, M. O., Kandler, K., Saeed, T., Piketh, S., Seibert, D., Williams, E., & Doussin, J.-F. (2017). Global scale variability of the mineral dust long-wave refractive index: A new dataset of in situ measurements for climate modeling and remote sensing. *Atmospheric Chemistry and Physics*, *17*(3), 1901–1929. https://doi.org/10.5194/acp-17-1901-2017

Dubovik, O., Holben, B., Eck, T. F., Smirnov, A., Kaufman, Y. J., King, M. D., Tanré, D., & Slutsker, I. (2002). Variability of Absorption and Optical Properties of Key Aerosol Types Observed in Worldwide Locations. *Journal of the Atmospheric Sciences*, *59*(3), 590–608. https://doi.org/10.1175/1520-0469(2002)059%253C0590:VOAAOP%253E2.0.CO;2

Dubovik, O., & King, M. D. (2000). A flexible inversion algorithm for retrieval of aerosol optical properties from Sun and sky radiance measurements. *Journal of Geophysical Research: Atmospheres*, *105*(D16), 20673–20696. https://doi.org/10.1029/2000JD900282

Dubovik, O., Sinyuk, A., Lapyonok, T., Holben, B. N., Mishchenko, M., Yang, P., Eck, T. F., Volten, H., Muñoz, O., Veihelmann, B., Van Der Zande, W. J., Leon, J., Sorokin, M., & Slutsker, I. (2006). Application of spheroid models to account for aerosol particle nonsphericity in remote sensing of desert dust. *Journal of Geophysical Research: Atmospheres*, *111*(D11), 2005JD006619. https://doi.org/10.1029/2005JD006619

Fu, G., Rietjens, J., Laasner, R., Van Der Schaaf, L., Van Hees, R., Yuan, Z., Van Diedenhoven, B., Hannadige, N., Landgraf, J., Smit, M., Knobelspiesse, K., Cairns, B., Gao, M., Franz, B., Werdell, J., & Hasekamp, O. (2025). Aerosol Retrievals From SPEXone on the NASA PACE Mission: First Results and Validation. *Geophysical Research Letters*, *52*(4), e2024GL113525. https://doi.org/10.1029/2024GL113525

Garrigues, S., Ades, M., Remy, S., Flemming, J., Kipling, Z., Laszlo, I., Parrington, M., Inness, A., Ribas, R., Jones, L., Engelen, R., & Peuch, V.-H. (2023). Impact of assimilating NOAA VIIRS aerosol optical depth (AOD) observations on global AOD analysis from the Copernicus Atmosphere Monitoring Service (CAMS). *Atmospheric Chemistry and Physics*, *23*(18), 10473–10487. https://doi.org/10.5194/acp-23-10473-2023

Gelaro, R., McCarty, W., Suárez, M. J., Todling, R., Molod, A., Takacs, L., Randles, C. A., Darmenov, A., Bosilovich, M. G., Reichle, R., Wargan, K., Coy, L., Cullather, R., Draper, C., Akella, S., Buchard, V., Conaty, A., Da Silva, A. M., Gu, W., … Zhao, B. (2017). The Modern-Era Retrospective Analysis for Research and Applications, Version 2 (MERRA-2). *Journal of Climate*, *30*(14), 5419–5454. https://doi.org/10.1175/JCLI-D-16-0758.1

Gliß, J., Mortier, A., Schulz, M., Andrews, E., Balkanski, Y., Bauer, S. E., Benedictow, A. M. K., Bian, H., Checa-Garcia, R., Chin, M., Ginoux, P., Griesfeller, J. J., Heckel, A., Kipling, Z., Kirkevåg, A., Kokkola, H., Laj, P., Le Sager, P., Lund, M. T., … Tsyro, S. G. (2021). AeroCom phase III multi-model evaluation of the aerosol life cycle and optical properties using ground- and space-based remote sensing as well as surface in situ observations. *Atmospheric Chemistry and Physics*, *21*(1), 87–128. https://doi.org/10.5194/acp-21-87-2021

Henne, S., Brunner, D., Oney, B., Leuenberger, M., Eugster, W., Bamberger, I., Meinhardt, F., Steinbacher, M., & Emmenegger, L. (2016). Validation of the Swiss methane

emission inventory by atmospheric observations and inverse modelling. *Atmospheric Chemistry and Physics*, *16*(6), 3683–3710. https://doi.org/10.5194/acp-16-3683-2016

Hess, M., Koepke, P., & Schult, I. (1998). Optical Properties of Aerosols and Clouds: The Software Package OPAC. *Bulletin of the American Meteorological Society*, *79*(5), 831–844. https://doi.org/10.1175/1520-0477(1998)079%253C0831:OPOAAC%253E2.0.CO;2

Inness, A., Ades, M., Agustí-Panareda, A., Barré, J., Benedictow, A., Blechschmidt, A.-M., Dominguez, J. J., Engelen, R., Eskes, H., Flemming, J., Huijnen, V., Jones, L., Kipling, Z., Massart, S., Parrington, M., Peuch, V.-H., Razinger, M., Remy, S., Schulz, M., and Suttie, M.: The CAMS reanalysis of atmospheric composition, Atmos. Chem. Phys., 19, 3515–3556, https://doi.org/10.5194/acp-19-3515-2019, 2019.

Moosmüller, H., Engelbrecht, J. P., Skiba, M., Frey, G., Chakrabarty, R. K., & Arnott, W. P. (2012). Single scattering albedo of fine mineral dust aerosols controlled by iron concentration. *Journal of Geophysical Research: Atmospheres*, *117*(D11). https://doi.org/10.1029/2011JD016909

Romshoo, B., Müller, T., Ahlawat, A., Wiedensohler, A., Haneef, M., Imran, M., Warsi, A. B., Mandariya, A. K., Habib, G., & Pöhlker, M. L. (2024). Significant contribution of fractal morphology to aerosol light absorption in polluted environments dominated by black carbon (BC). *Npj Climate and Atmospheric Science*, *7*(1), 87.

Ryder, C. L., Marenco, F., Brooke, J. K., Estelles, V., Cotton, R., Formenti, P., McQuaid, J. B., Price, H. C., Liu, D., Ausset, P., Rosenberg, P. D., Taylor, J. W., Choularton, T., Bower, K., Coe, H., Gallagher, M., Crosier, J., Lloyd, G., Highwood, E. J., & Murray, B. J. (2018). Coarse-mode mineral dust size distributions, composition and optical properties from AER-D aircraft measurements over the tropical eastern Atlantic. *Atmospheric Chemistry and Physics*, *18*(23), 17225–17257. https://doi.org/10.5194/acp-18-17225-2018

Saha, S., Moorthi, S., Pan, H.-L., Wu, X., Wang, J., Nadiga, S., Tripp, P., Kistler, R., Woollen, J., Behringer, D., Liu, H., Stokes, D., Grumbine, R., Gayno, G., Wang, J., Hou, Y.-T., Chuang, H., Juang, H.-M. H., Sela, J., … Goldberg, M. (2010). The NCEP Climate Forecast System Reanalysis. *Bulletin of the American Meteorological Society*, *91*(8), 1015–1058. https://doi.org/10.1175/2010BAMS3001.1

Schutgens, N., Dubovik, O., Hasekamp, O., Torres, O., Jethva, H., Leonard, P. J. T., Litvinov, P., Redemann, J., Shinozuka, Y., De Leeuw, G., Kinne, S., Popp, T., Schulz, M., & Stier, P. (2021). AEROCOM and AEROSAT AAOD and SSA study – Part 1: Evaluation and intercomparison of satellite measurements. *Atmospheric Chemistry and Physics*, *21*(9), 6895–6917. https://doi.org/10.5194/acp-21-6895-2021

Schutgens, N. A. J.: Site representativity of AERONET and GAW remotely sensed aerosol optical thickness and absorbing aerosol optical thickness observations, Atmos. Chem. Phys., 20, 7473–7488, https://doi.org/10.5194/acp-20-7473-2020, 2020.

Snow, T., & Scheick, J. (2023, December 31). CryoCloud update for ICESat-2 Science Team (July 2023). Zenodo. https://doi.org/10.5281/zenodo.10445824

Takemura, T., Nakajima, T., Dubovik, O., Holben, B. N., & Kinne, S. (2002). Single-Scattering Albedo and Radiative Forcing of Various Aerosol Species with a Global Three-Dimensional Model. Journal of Climate, 15(4), 333–352. https://doi.org/10.1175/1520-0442(2002)015%253C0333:SSAARF%253E2.0.CO;2

Tsikerdekis, A., Schutgens, N. A. J., & Hasekamp, O. P. (2021). Assimilating aerosol optical properties related to size and absorption from POLDER/PARASOL with an ensemble data assimilation system. Atmospheric Chemistry and Physics, 21(4), 2637–2674. https://doi.org/10.5194/acp-21-2637-2021

Wang, J., Wang, J., Cai, R., Liu, C., Jiang, J., Nie, W., Wang, J., Moteki, N., Zaveri, R. A., Huang, X., & others. (2023). Unified theoretical framework for black carbon mixing state allows greater accuracy of climate effect estimation. Nature Communications, 14(1), 2703.

Woodward, S. (2001). Modeling the atmospheric life cycle and radiative impact of mineral dust in the Hadley Centre climate model. Journal of Geophysical Research: Atmospheres, 106(D16), 18155–18166. https://doi.org/10.1029/2000JD900795

Xian, P., Reid, J. S., Ades, M., Benedetti, A., Colarco, P. R., da Silva, A., Eck, T. F., Flemming, J., Hyer, E. J., Kipling, Z., Rémy, S., Sekiyama, T. T., Tanaka, T., Yumimoto, K., & Zhang, J. (2024). Intercomparison of aerosol optical depths from four reanalyses and their multi-reanalysis consensus. Atmospheric Chemistry and Physics, 24(10), 6385–6411. https://doi.org/10.5194/acp-24-6385-2024

Yin, X., Dai, T., Schutgens, N. A. J., Goto, D., Nakajima, T., & Shi, G. (2016). Effects of data assimilation on the global aerosol key optical properties simulations. Atmospheric Research, 178–179, 175–186. https://doi.org/10.1016/j.atmosres.2016.03.016

Zeng, L., Tan, T., Zhao, G., Du, Z., Hu, S., Shang, D., & Hu, M. (2024). Overestimation of black carbon light absorption due to mixing state heterogeneity. Npj Climate and Atmospheric Science, 7(1), 2.

Appendix

A. Aerosol specie contribution and correlation in CAMS

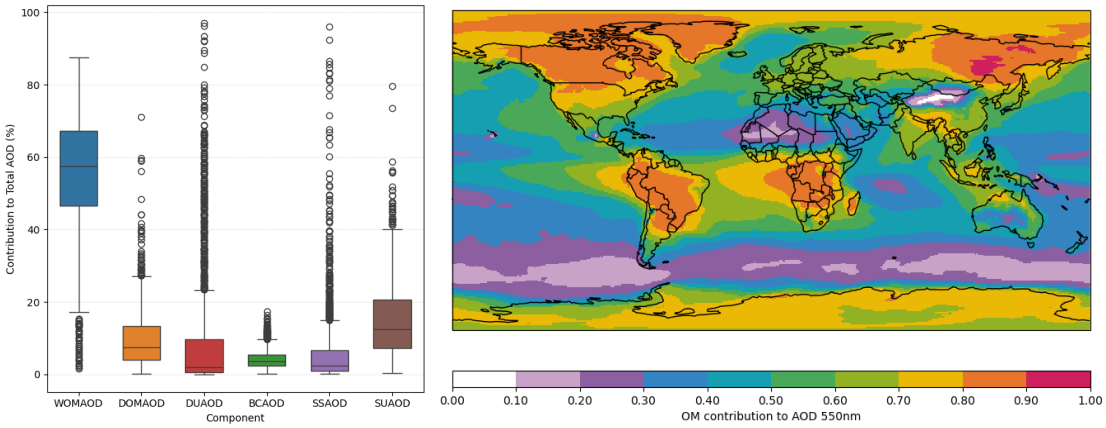

Figure A-1 - Relative contribution of the individual AOD component for the total AOD at 550nm from the IFS data for AERONET sites (left). Yearly (2023&2024) OM AOD contribution to the total AOD at 550nm (right).

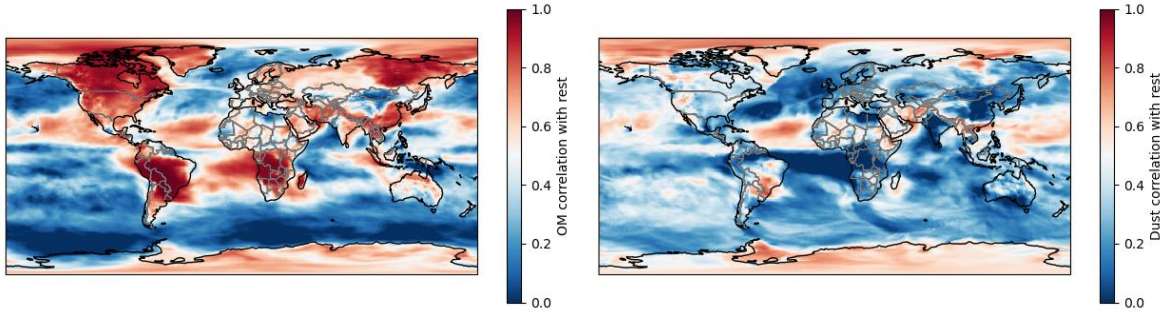

Figure A-2 - The Pearson correlation R (color) between OM AOD (left) and dust AOD (right) and the AOD contribution from the other aerosols (AOD at 550 nm).

B. Relative humidity on SSA and ASY

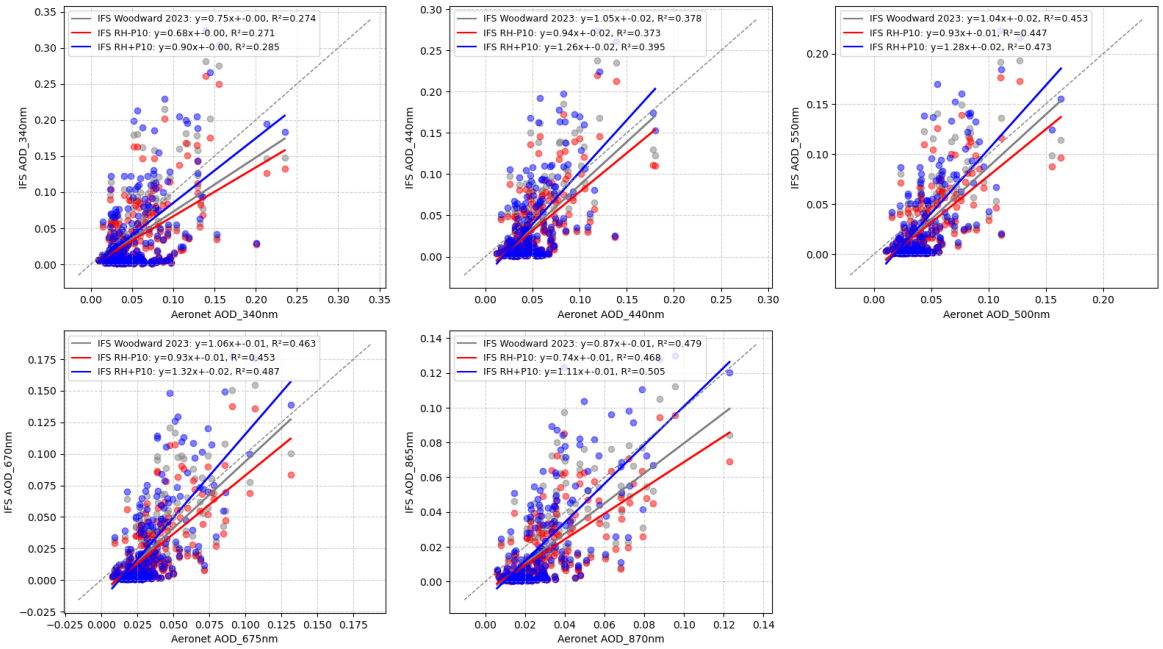

Figure B-1 - Comparison between AERONET AOD and OOPP model simulations at five wavelengths (340, 440, 500, 675, and 870 nm) for sea salts dominated locations in 2023. Colours follow the same scheme as in Figures 4-8.

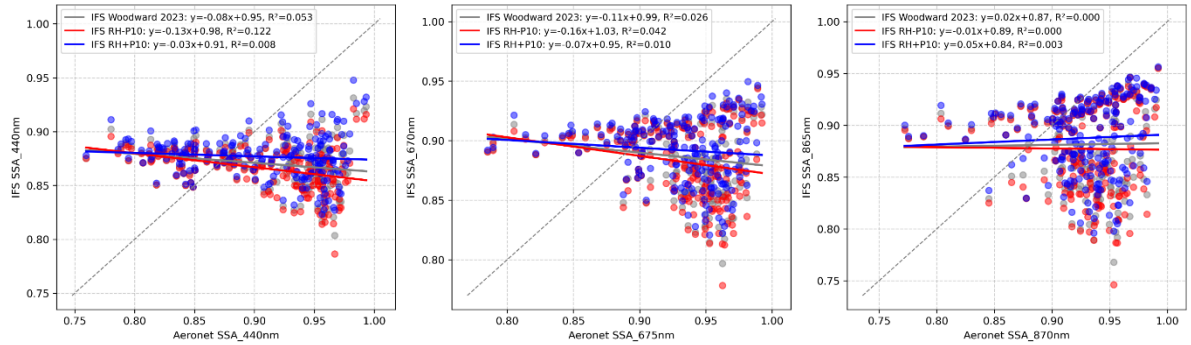

Figure B-2 - Comparison between AERONET SSA and OOPP model simulations at three wavelengths (440, 675, and 870 nm) for 2023. Colors follow the same scheme as in Figures 4-8.

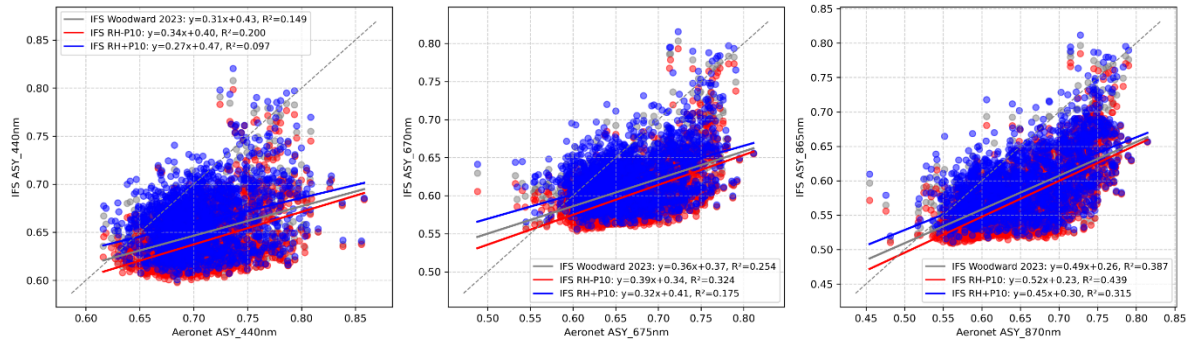

Figure B-3 - Comparison between AERONET ASY and OOPP model simulations at three wavelengths (440, 675, and 870 nm) for 2023. Colors follow the same scheme as in Figures 4-8.

C. Sea salt experiment

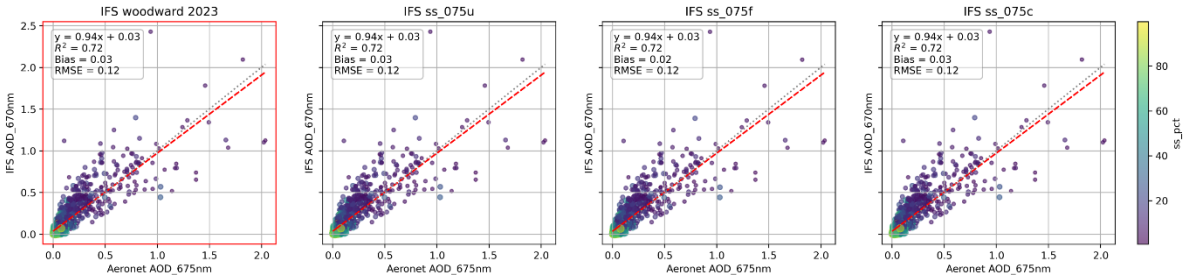

Figure C-1 - Comparison between AERONET AOD and OOPP model simulations AOD at 675 nm for all sites in 2023. Scatter points are colored and sized according to the relative contribution of sea salt.

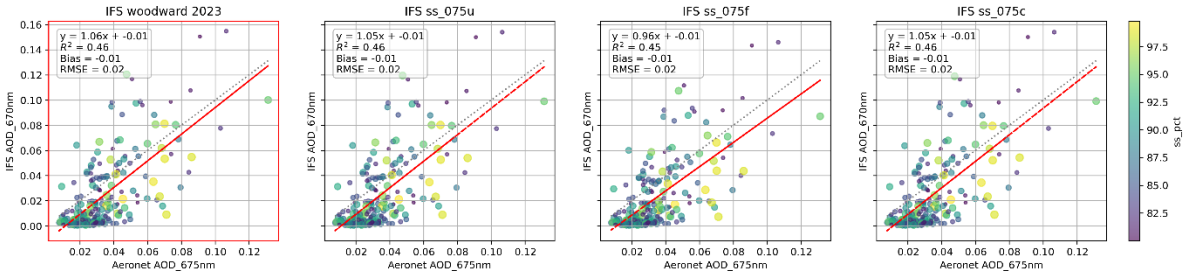

Figure C-2 - Comparison between AERONET AOD and OOPP model simulations AOD at 675 nm for sea salts dominated points in 2023. Scatter points are colored and sized according to the relative contribution of sea salt.

D. spectral error and correlation comparing to SPEXone

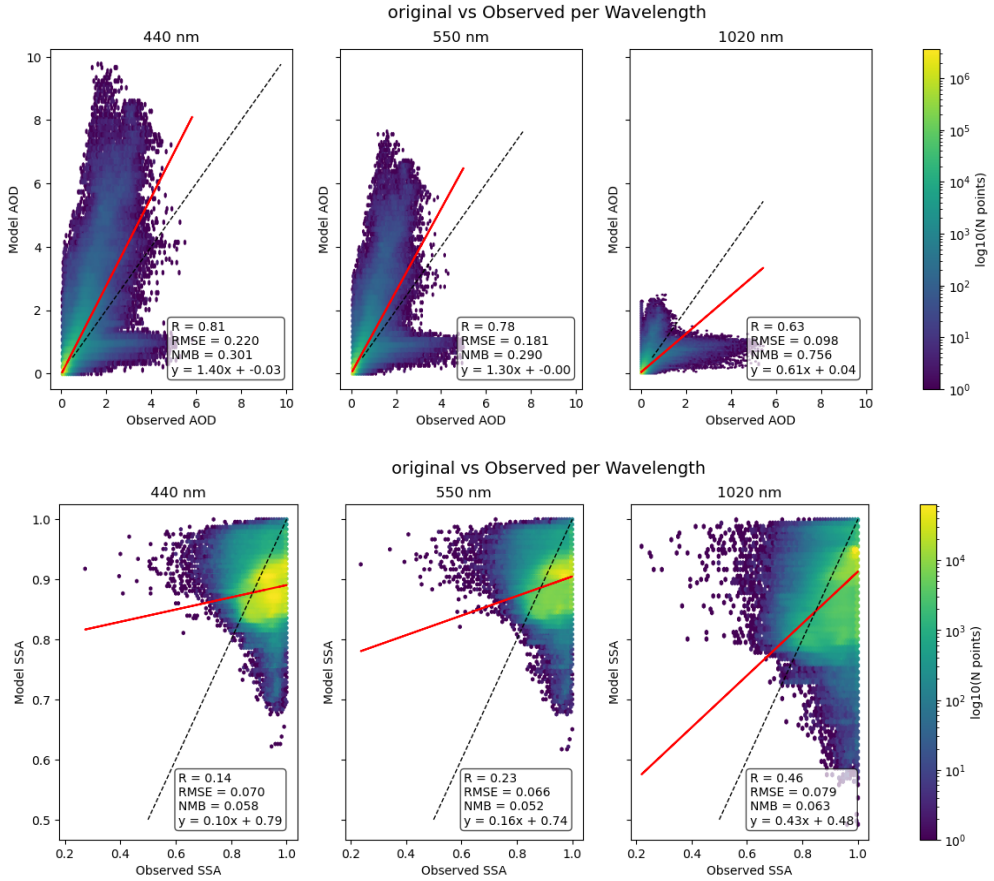

Figure D-1 - Scatter density plot of ungridded comparisons of SPEXone and Modelled AOD (top) and SSA which was filtered by AOD at 550nm >0.3 (bottom) with Pearson correlation R, RMSE, NMB and linear regression fit as red line. Color represents the density of points.

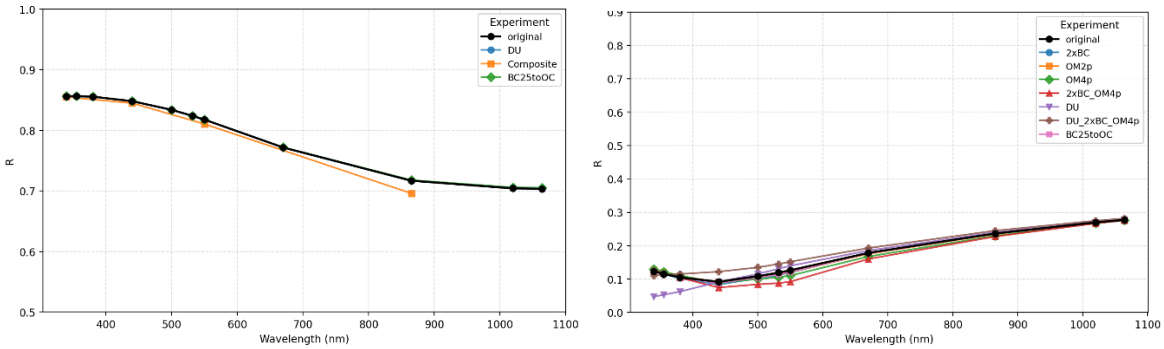

Figure D-2 - Monthly gridded AOD Pearson correlation(left), Dubovik in blue, composite and 25% BC to OC (BC25toOC) experiments; Right of SSA correlation in all experiments of AOD and in addition OM2p. OM4p, 2xBC and combination of them.

E. SSA experiment - AERONET

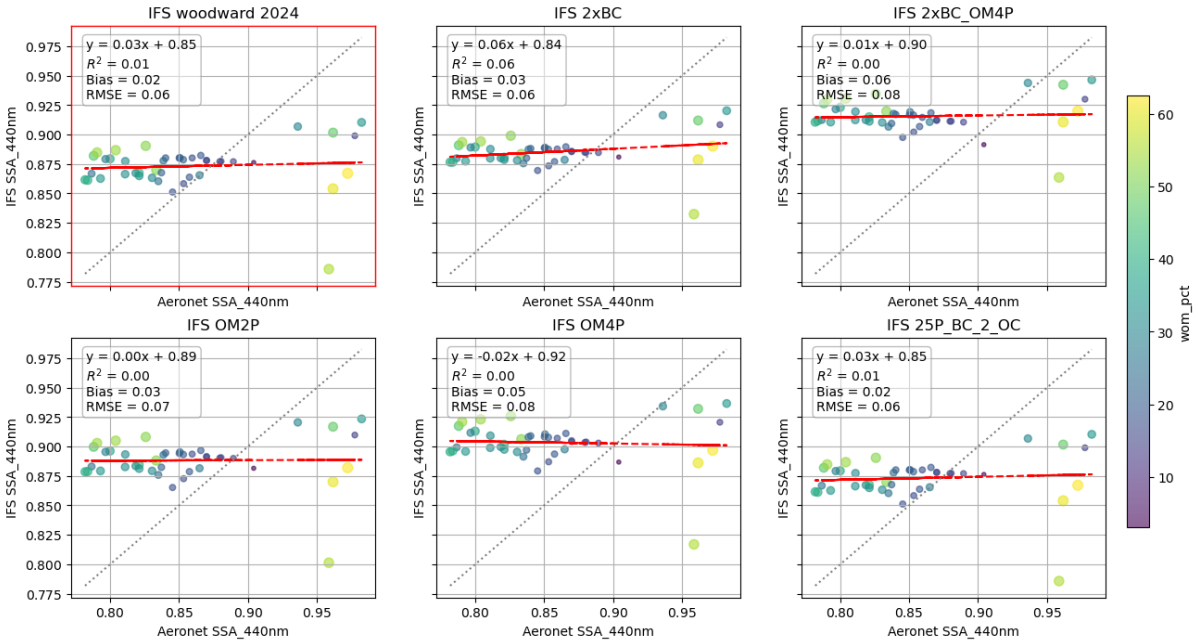

Figure E-1 - Comparison between AERONET observations and OOPP model simulations for SSA experiments (described in Table 2) at 440 nm for 2024. Scatter points are colored and sized according to the relative contribution of WOM.

F. Dust representation

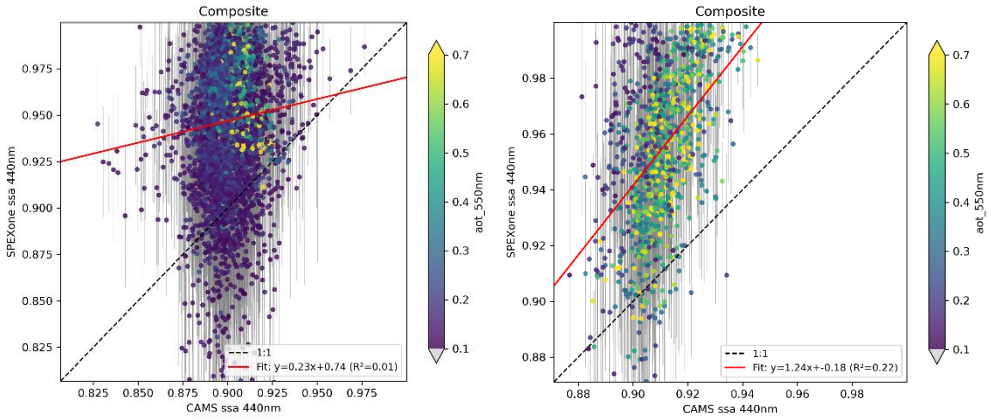

Figure F-1 – Comparison of SSA at 440 nm between CAMS reanalysis and SPEXone for the regions of Sahara (left) and Northeast India (right), where the model used the composite dust optical scheme. Each point is a 1°x1° monthly regridded SPEXone median observation, with the bar representing standard deviation with collocated modelled SSA. The colour is SEPXone AOD at 550nm.

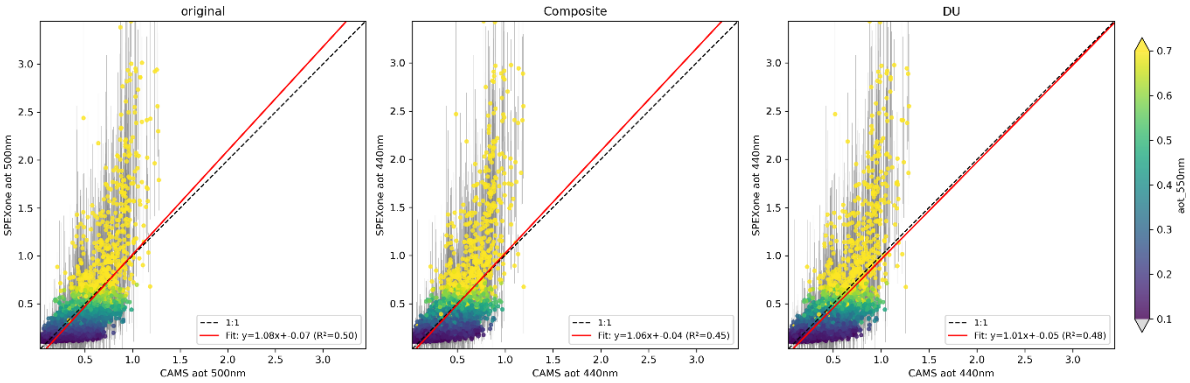

Figure F-2 Sahara AOD 550 of composite dust optical scheme. Each points are 1x1 degree monthly regridded SPEXone observation median with bar representing standard deviation with collocated modelled SSA. The colour is SEPXone AOD at 550nm

Document History

Version	Author(s)	Date	Changes
0.1	Jessie Zhang, Xinya Liu, Janot Tokaya, Arjo Segers	24/11/2025	Initial version for internal review.
1.0	Jessie Zhang, Xinya Liu, Janot Tokaya, Arjo Segers	17/12/2025	Final version.

Internal Review History

Internal Reviewers	Date	Comments
Pavel Litvinov (GRASP)	Nov 2025	
Vincent Huijnen (KNMI)	Dec 2025	
Thanos Tsikerdekis (KNMI)	Dec 2025	